A Model for the Complete Radial Structure of the Tropical Cyclone Wind Field. Part II: Wind Field Variability

DANIEL R. CHAVAS AND NING LIN

Department of Civil and Environmental Engineering, Princeton University, Princeton, New Jersey

(Manuscript received 6 July 2015, in final form 25 March 2016)

ABSTRACT

Part I of this work developed a simple physical model for the complete radial structure of the low-level azimuthal wind field in a tropical cyclone that compared well with observations. However, wind field variability in the model is tied principally to its external parameters given by the maximum wind speed and the radius of maximum wind, the latter of which lacks a credible independent physical model for its variability. Here the authors explore the modes of variability that arise from the alternative specification of the model, which takes the outer radius in lieu of the radius of maximum wind. Nondimensionalization of the model reveals two theoretical modes of structural variability in absolute angular momentum that are shown to closely match observations. These two modes correspond to three modes of wind field variability associated with variations in intensity, outer storm size, and latitude. These wind field modes are demonstrated to mirror the dominant modes of variability found in nature, in particular the intrastorm variation of inner-core structure and the interstorm variation of overall storm size. In combination, the model offers a credible physical solution for the complete time-dependent tropical cyclone wind field in conjunction with the external specification of intensity, outer size, and latitude. More broadly, the model offers theoretical and conceptual insight into the nature of the tropical cyclone wind field, including the oft-conflated terms ''size'' and ''structure'' and their distinct variabilities.

1. Introduction

Variability in the low-level circulation of the tropical cyclone is known to possess certain curious traits. The wind fields at small and large radii, broadly defined, appear to vary nearly independently of one another in nature (Weatherford and Gray 1988). In the turbulent inner core, where short-time-scale variability is common (e.g., Tang and Emanuel 2012; Smith 1980; Sitkowski et al. 2011), changes in intensity are commonly associated with anticorrelated changes in the radius of maximum winds (e.g., Demuth et al. 2006; Kossin et al. 2007; Vigh et al. 2012), which follows from basic principles of angular momentum conservation. In contrast, the stable outer circulation is largely agnostic to the vagaries of the inner core, a feature noted in observations (Merrill 1984; Lee et al. 2010; Chavas and Emanuel 2010; Chan and Chan 2012) and numerical models (Rotunno and Bryan 2012; Chavas and Emanuel 2014) and that is consistent with existing theory that permits variability in the radius of maximum wind relative to a fixed outer radius of vanishing wind (Emanuel 1986; Emanuel and Rotunno 2011). Meanwhile, though the outer circulation is stable in time, its absolute length scale is known to vary substantially from storm to storm [e.g., the radius of $12\,\mathrm{m\,s^{-1}}$ (denoted r_{12}) (Chavas and Emanuel 2010; Chavas et al. 2016), 5 knots ($1\,\mathrm{kt} = 0.51\,\mathrm{m\,s^{-1}}$) (Knaff et al. 2014), or outermost closed isobar (Merrill 1984)].

Despite advances in our understanding of wind field variability, there remains the need for a credible theoretical model for the wind field capable of reproducing these known behavioral characteristics and uniting them under a common physical framework. In particular, the wind field is fundamentally a manifestation of the radial distribution of absolute angular momentum (e.g., Chan and Chan 2013, 2014, 2015), which must increase monotonically with radius (for inertial stability) from zero at the center and whose only source lies at larger radii. Consequently, angular momentum is implicitly correlated in radius, as any local increase (e.g., storm

Corresponding author address: Daniel R. Chavas, Purdue University, Department of Earth, Atmospheric, and Planetary Sciences, 550 Stadium Mall Drive, HAMP 3221, West Lafayette, IN 47907.
E-mail: drchavas@gmail.com

DOI: 10.1175/JAS-D-15-0185.1

intensification) requires import from larger radius. More generally, the relative angular momentum of the storm circulation is ultimately drawn from Earth's planetary angular momentum at large radii as its source. Thus, we seek a model specifically for how absolute angular momentum decreases toward smaller radius (i.e., "structure"). As a first step to this end, Chavas et al. (2015, hereafter Part I) developed a simple physical model for the complete radial structure of the low-level absolute angular momentum field, and thus azimuthal wind field, in a tropical cyclone. The model is given by the juxtaposition of preexisting solutions for absolute angular momentum in the inner ascending region (Emanuel and Rotunno 2011) and the outer descending region (Emanuel 2004) and was shown to compare well against observations when given the maximum wind V_m and radius of maximum wind r_m as input parameters.

Beyond directly reproducing the radial structure, though, one further seeks a model for its space–time variability. In the model as presented in Part I, much of the variability of interest is implicit within its input parameters (V_m, r_m), thereby necessitating external models for their respective variabilities. In the case of V_m, credible physically based models exist (Tang and Emanuel 2012; DeMaria and Kaplan 1994). However, no such model currently exists for r_m that is independent of a second radial length scale. Moreover, r_m poses difficulties for its estimation in observations owing to the aforementioned turbulent nature of the inner core of a tropical cyclone and its associated asymmetries, particularly given its propensity for discontinuous jumps due to eyewall replacement cycles (Sitkowski et al. 2011), as well as a lack of consistent, high-quality inner-core wind observations (e.g., Vigh et al. 2012). Finally, r_m requires high radial resolution in order to be confidently represented in a numerical model ($\leq$4 km; e.g., Chavas and Emanuel 2014), which is of particular significance in the context of climate models, for which such resolutions are currently computationally expensive. In contrast, measures of the outer circulation are largely immune to such problems, particularly for radii of low-to-moderate wind speeds (Knaff and Zehr 2007; Chavas and Emanuel 2010; Knutson et al. 2015), and carry the significant added benefit of being largely independent of intensity, unlike r_m. The implication, then, is that one may potentially bypass r_m, and even predict r_m, if the radial structure can instead be specified using a metric of outer storm size. Though statistical relationships between r_m and metrics of outer size from historical data may be employed, a physical model is preferable, especially if it permits more general analysis of relationships at all radii. Importantly, beyond practical benefits, such an "outside in" perspective is theoretically appealing given that the angular momentum of the storm circulation necessarily originates from large radii as discussed above.

Conveniently, the complete model developed in Part I offers such a path forward, as it may alternatively be specified using the outer radius of vanishing wind r_0 in lieu of r_m. Here we demonstrate that this alternative specification can reproduce the characteristic modes of variability of the tropical cyclone wind field in nature. Section 2 revisits the theory of Part I in the context of wind field variability and explores the fundamental modes of variability intrinsic to the model. Section 3 compares theoretical variability to observations. Section 4 discusses implications of the model for both understanding and modeling the wind field. Finally, section 5 synthesizes key conclusions across both parts of this work.

2. Model variability

a. Theory

We begin with a brief review of the theory presented in Part I, with the model rephrased nondimensionally for the purposes of analyzing wind field variability. Part I developed a solution for the complete radial profile of the azimuthal wind at the top of the boundary layer by mathematically merging two distinct, preexisting theoretical solutions that apply to the inner ascending and outer descending regions of a tropical cyclone, respectively. These solutions are phrased in terms of absolute angular momentum per unit mass, given by

$$M = rV + \frac{1}{2} fr^2, \tag{1}$$

where r is radius, V is the azimuthal wind speed, and f is the Coriolis parameter.

First, the inner ascending solution (Emanuel and Rotunno 2011) links the radial distribution of M at the top of the boundary layer to the radial distribution of the outflow temperature. The result is given by

$$\left(\frac{M}{M_m}\right)^{2-C_k/C_d} = \frac{2(r/r_m)^2}{2-(C_k/C_d)+(C_k/C_d)(r/r_m)^2}, \tag{2}$$

where

$$M_m = r_m V_m + \frac{1}{2} fr_m^2 \tag{3}$$

is the angular momentum at the radius of maximum wind and C_k/C_d is the ratio of the exchange coefficients of enthalpy and momentum. As Eq. (2) is an asymptotic approximation to the full solution, the parameters r_m and V_m exactly equal the radius of maximum wind and

maximum wind speed only in the high-vorticity limit ($V_m/fr_m \gg 1$). As detailed in Part I, C_k/C_d in this model is taken as an increasing function of V_m, spanning the range [0.4, 1], based on best-fit estimates of the inner-core angular momentum profile beyond r_m using the HWind observational database (Powell et al. 1998). Though the range of values of C_k/C_d is of the correct order of magnitude, its increase with wind speed disagrees with existing observational estimates and thus it is considered to be a tunable parameter; the reader is referred to Part I for further discussion. The sensitivity of the model to the value of C_k/C_d is explored in the subsequent section.

Second, the outer descending solution (Emanuel 2004) links the radial gradient of M at the top of the boundary layer to the thermodynamics of the quiescent free troposphere in radiative–subsidence balance. The solution is given by

$$\frac{\partial M}{\partial r} = \frac{2C_d}{W_{\text{cool}}} \frac{(rV)^2}{r_0^2 - r^2}, \tag{4}$$

where r_0 is the outer radius of vanishing wind, C_d is the surface drag coefficient, and W_{cool} is the magnitude of the radiative-subsidence rate in the free troposphere. We reexpress this solution in a more convenient form by first rewriting the relative angular momentum term rV using the definition of M [Eq. (1)] and then nondimensionalizing r by r_0 and M by its value at r_0, given by

$$M_0 = \frac{1}{2} f r_0^2. \tag{5}$$

The result is

$$\frac{\partial \tilde{M}}{\partial \tilde{r}} = \gamma \frac{(\tilde{M} - \tilde{r}^2)^2}{1 - \tilde{r}^2}, \tag{6}$$

where $\tilde{r} = r/r_0$ and $\tilde{M} = M/M_0$ and the lone free parameter is given by

$$\gamma = \frac{f r_0}{W_{\text{cool}}/C_d}. \tag{7}$$

This form combines all free parameters in the solution into one nondimensional parameter γ, which comprises the ratio of two distinct velocity scales given by fr_0 and W_{cool}/C_d. The former is a storm-specific free parameter that depends on the outer size and latitude of a given storm at a given time, while the latter may be considered as an environmental free parameter that does not vary significantly from storm to storm. As detailed in Part I, W_{cool} is taken as a constant equal to its estimated climatological value of $2\,\text{mm}\,\text{s}^{-1}$, and C_d is taken as a function of V fit to the data of Donelan et al. (2004). Note that if C_d is held constant with wind speed, then γ may be truly treated as a single free parameter. However, the dependence of C_d on absolute wind speed necessarily decomposes γ into two distinct parameters given by its constituent velocity scales, W_{cool}/C_d and fr_0. This behavior arises because the solution for the absolute wind speed is given by Eq. (4) where fr_0 does not appear; as a result, the wind speed dependence applied to W_{cool}/C_d cannot be generalized to apply to γ (i.e., for variable C_d, equivalent variations in $1/W_{\text{cool}}$ and fr_0 produce similar but not identical outcomes). Additionally, we note that the indeterminate form of the dimensional solution at $r = r_0$ is eliminated in the formulation given by Eq. (6): substitution of $\tilde{M}(\tilde{r} = 1) = 1$ in Eq. (6) leads to $\tilde{M}'(\tilde{r} = 1) = \gamma(1 - \tilde{r}^2) = 0$. To the authors' knowledge, Eq. (6) still cannot be solved analytically. Equation (6) will be leveraged in the analysis of structural variability presented below.

Finally, the inner and outer solutions can be directly merged at the merge radius r_a, which is unique for a given set of parameters over a wide range of all parameter values as described in Part I. This fact may be understood geometrically, as Eq. (2) is concave down and approaches constant angular momentum in the limit of large radius, while the solution to Eq. (6) is concave up and approaches constant angular momentum in the limit of small radius. Note that each solution for the distribution of M is nondimensionalized here with respect to its value at distinct radii: r_m for the inner solution and r_0 for the outer solution. This distinction provides theoretical grounding for the aforementioned tendency for the inner core of tropical cyclones to vary relative to a stable outer circulation (Weatherford and Gray 1988), which is analyzed in much greater detail below. More significantly, we may exploit the form of these equations to quantify the interrelationship between the inner and outer regions of the storm. The simplest quantity representative of this relationship is given by the ratio of the angular momentum at the radius of maximum wind to that at the outer radius, M_m/M_0. One may rewrite this ratio as

$$\frac{M_m}{M_0} = \frac{M_m}{M_a} \frac{M_a}{M_0}, \tag{8}$$

where M_a is the angular momentum at the merge radius r_a. The inner model of Eq. (2) dictates that $M_m/M_a = \mathscr{F}_1(V_m, C_k/C_d)$, where the exact functional relationship arises from the reciprocal of Eq. (2) and we specify V_m in lieu of r_m, as V_m is the most common quantity of interest in observations and models and good estimates of its value are frequently available in operations (as discussed

in Part I). Meanwhile, the outer model of Eq. (6) is conveniently phrased in terms of M/M_0, which, in combination with the outer boundary condition $\tilde{M}(\tilde{r}=1)=1$, dictates that $M_a/M_0=\mathscr{F}_2(fr_0, W_{\rm cool}/C_d)$. Thus, Eq. (8) gives

$$M_m/M_0=\mathscr{F}(V_m, fr_0; C_k/C_d, W_{\rm cool}/C_d), \qquad (9)$$

where the external parameters have been separated by the nature of their variability: V_m and fr_0 are storm-specific parameters that both vary significantly from storm to storm and within the storm life cycle, while C_k/C_d in the inner region and $W_{\rm cool}/C_d$ in the outer region are largely environmental parameters that are not specific to a given storm. Note that (r_a, M_a) are internal parameters and so are implicitly dependent on the same set of external parameters. Moreover, fr_0 and $W_{\rm cool}/C_d$ impose different effects on (r_a, M_a) and thus must be treated as distinct parameters in the merged model even for fixed C_d.

Given the presence of the outer radius r_0 as an important parameter in the model, we briefly discuss some important considerations regarding its interpretation. As discussed in Part I, the outer solution is specified with a single length scale, which need not be r_0 itself. Once the solution is specified with a given wind radius (e.g., r_{12}), error in the model prediction of another wind radius (e.g., r_0, r_5, r_{15}) indicates error in some underlying assumption of the model (e.g., $W_{\rm cool}$); other wind radii, including r_0, are not independent. Part I demonstrated that this solution can successfully capture the broad outer circulation of the system, though because of data limitations the solution was not tested at very small wind speeds in the vicinity of r_0 itself. Even in the presence of perfect data coverage, direct testing of the model prediction of r_0 is complicated by the fact that the large-scale circulation in which a given storm is embedded may project onto the azimuthal-mean azimuthal wind, which will impose large biases on the precise radius at which the storm circulation is perceived to vanish (e.g., for a storm embedded in a large-scale trough, the azimuthal wind will only vanish at the very large radius at the edge of the trough). As a result, the true r_0 of the storm circulation is not readily defined directly from the full wind field unless the storm circulation is perfectly separated from the environmental flow. Instead, the outer structural model presents a dynamically based prediction of the value of r_0 that is constrained by its required consistency with the model at radii inside of r_0, where the model performs well (cf. Part I). Thus, though continued investigation of the true value of r_0 in nature is of scientific interest [and has recently been explored in Reed and Chavas (2015)], it is not essential to the validity of the model nor the analysis of its behavior presented here. It is noted, however, that an alternative wind radius serves as a practical but not a theoretical substitute for r_0: though the solution may be specified using this length scale in lieu of r_0, thereby replacing r_0 as the size parameter, the solution itself depends specifically on r_0 via Eq. (7). As such, r_0 is a fundamental theoretical quantity even if it need not be directly specified.

b. Modes of variability

As noted in Part I, given values for the environmental parameters C_k/C_d in the inner region and $W_{\rm cool}$ and C_d in the outer region (section 2a), the merged solution may be fully specified with either of two pairs of storm parameters: (V_m, r_m) or (V_m, r_0). Part I demonstrated that the resulting model radial structure compares well to observations for the simplest case of input (V_m, r_m), indicating that the model can largely capture the full radial wind structure of tropical cyclones in nature. Following from the theoretical framework presented above, we now seek to explore the nature of wind field variability that arises from the alternative specification with (V_m, r_0), in which r_m is implicitly predicted by the model. We focus principally on the modes of variability corresponding to variation of the two storm-specific parameters, V_m and fr_0, identified in the theory.

First, Fig. 1 displays model variability associated with variations in V_m at constant fr_0, with the result presented in nondimensional M space[1] ($\tilde{M}$ vs $\tilde{r}$; Fig. 1a) alongside the implicit mode of wind field variability in dimensional V space (V vs r; Fig. 1b). As V_m increases, angular momentum surfaces at small and intermediate radii shift radially inward while outer region angular momentum surfaces remain fixed. The inward contraction of M surfaces is expected, as intensification equates to a local increase in angular momentum, whose surfaces necessarily must come from larger radii following angular momentum conservation principles. Note that the merge point also contracts inward, indicating contraction of the radius of persistent deep convection as the outer model occupies an increasingly large fraction of the radial profile. Corresponding values of M_m/M_0 decrease rapidly from 0.15 at low intensity ($V_m=15\,{\rm m\,s^{-1}}$) and then more gradually, becoming nearly constant at approximately 0.074 above $35\,{\rm m\,s^{-1}}$ and even increasingly slightly to 0.075 at high intensity. Meanwhile, r_m continues to decrease with intensification relative to the fixed r_0. Figure 1 also shows the case of fixed $C_k/C_d=0.5$

[1] Both f and r_0 are fixed, and thus variability in $\tilde{M}$ space and M space are equivalent.

(dashed line, inset), in which M_m/M_0 continues to decrease gradually with intensification to a value of 0.057 for $V_m = 65\,\mathrm{m\,s^{-1}}$. The increase in C_k/C_d with intensity translates to a more rapid sharpening of the inner model solution, which acts to shift the inner solution outward to allow for merging with the outer solution, thereby offseting the reduction of M_m associated with intensification if C_k/C_d were held fixed. As such, the value of C_k/C_d affects not only structure but also the absolute radius of the inner-core wind field in this model. More generally, the model implicitly allows for large variations in the inner-core wind field (r_m, V_m) relative to a stable outer wind field, precisely as was observed by Weatherford and Gray (1988).

Second, Fig. 2 displays model variability associated with variations in fr_0 at constant V_m, with the result presented in $\tilde{M}$ space (Fig. 2a) alongside the two implicit modes of wind field variability in V space characterized by independent variations in r_0 (Fig. 2b) and f (Fig. 2c). Increasing fr_0 shifts the nondimensional angular momentum profile downward, an indication of a more rapid fractional loss of angular momentum (relative to M_0) inward of r_0. Corresponding values of M_m/M_0 also decrease with increasing fr_0 at a rate of approximately 40% per doubling of fr_0, indicating from a Lagrangian perspective that, all else equal, a boundary layer air parcel in a larger or higher-latitude storm loses a larger fraction of its initial angular momentum while in transit from the outer radius to the radius of maximum wind. This mode of variability in $\tilde{M}$ space translates to two distinct modes in V space. First, variation in r_0 at constant f corresponds to changes in overall storm size, such that the entire storm structure is rescaled monotonically, though nonuniformly, in radius according to the model physics. Second, variation in f at constant r_0 corresponds to a subtler change in storm structure as a result of changes in latitude at constant intensity and size, in which for increasing f the wind field gradually expands radially outward, but relative to a fixed outer radius. This expansion is most pronounced at intermediate radii, as r_0 is fixed and changes in r_m are modest. Notably, an increase in f corresponds to a decrease in M_m/M_0 despite a concurrent increase in r_m itself, as the small increase in M_m (which is independent of f for a reasonably intense storm, where $M_m \approx r_m V_m$) does not offset the larger increase in M_0 accompanying the increase in f. Note that the magnitude of variations in r_0 and f are identical in Figs. 2b and 2c, indicating that the wind field is much less sensitive to variations in f than to equivalent variations in r_0. This result can be understood simply from the definition of M_m/M_0 in the high-vorticity limit, which for given values of fr_0 and V_m yields $r_m \propto fr_0^2/V_m$. Thus, a doubling of r_0 yields a value of r_m that is twice as large as its value for double f (e.g., for the base case of Figs. 1 and 2, a doubling of f increases r_m from 16.2 to 19.9 km, while a doubling of r_0 gives 39.8 km).

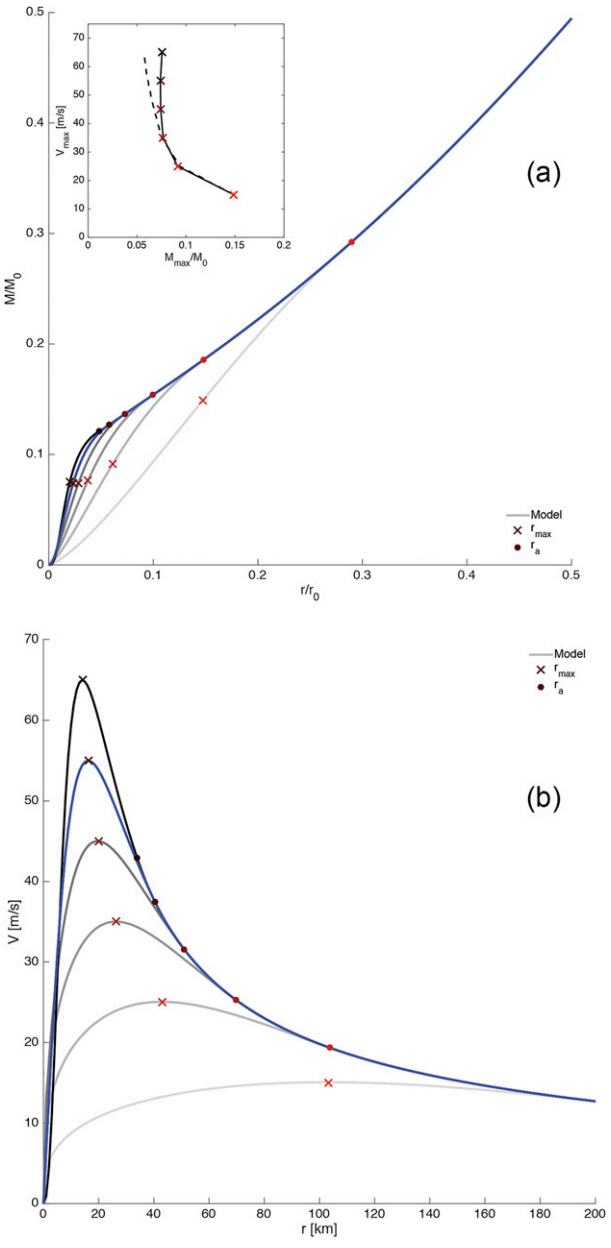

FIG. 1. Model variability associated with varying V_m at constant fr_0, displayed in terms of (a) nondimensional angular momentum and (b) wind speed. Parameter values: $V_m \in [15, 65]$ (light to dark); $fr_0 = 35\,\mathrm{m\,s^{-1}}$, corresponding to, e.g., $r_0 = 700\,\mathrm{km}$ and $f = 5 \times 10^{-5}\,\mathrm{s^{-1}}$. Markers denote r_m (crosses) and r_a (dots). Inset in (a) depicts M_m/M_0 as a function of V_m; the case of fixed $C_k/C_d = 0.5$ is also shown (dashed). Solution shown in blue is common to both this figure and Fig. 2. All $\tilde{M}$ curves converge by definition to (1, 1).

In summary, three fundamental modes of wind field variability (V_m, r_0, f) arise from the two modes of

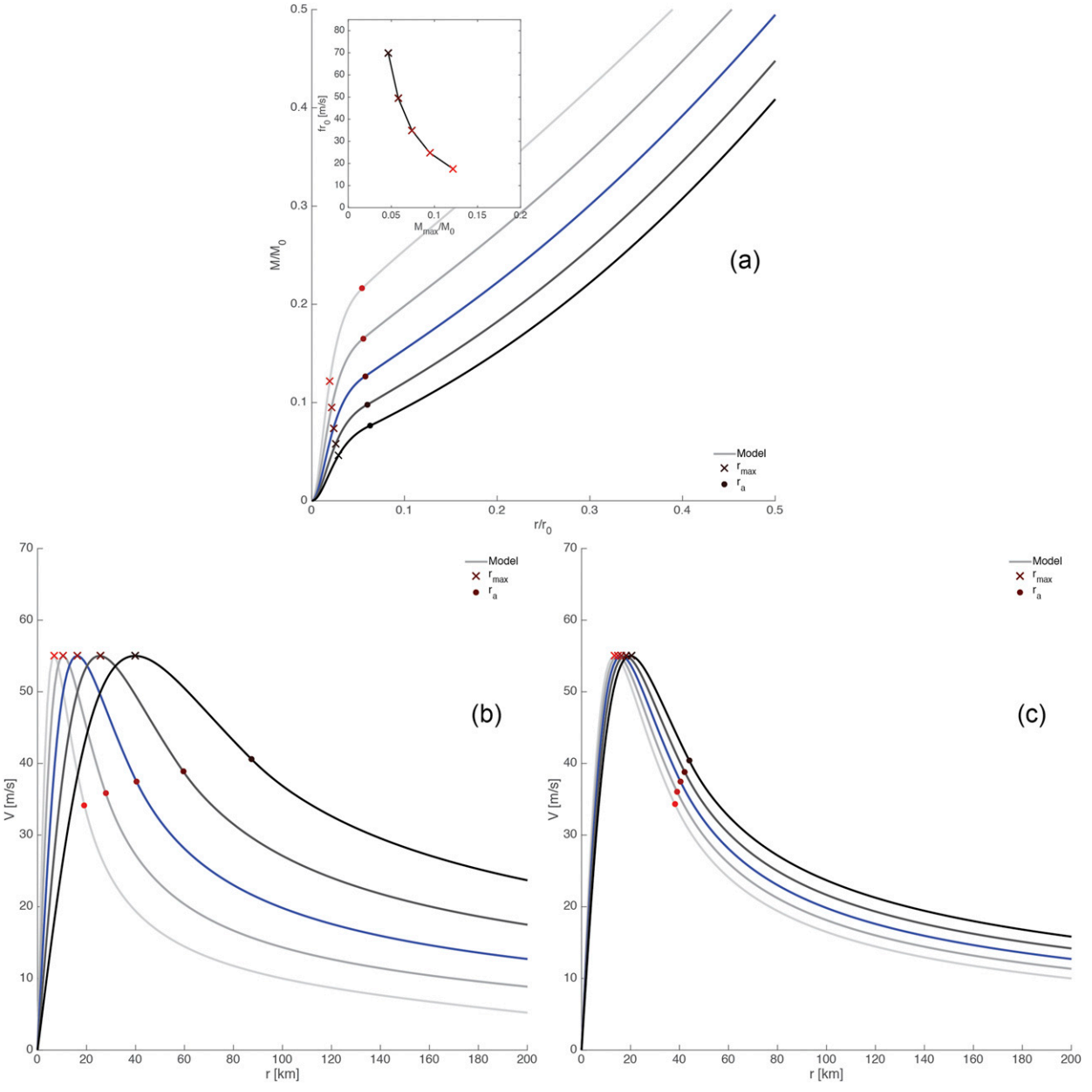

FIG. 2. As in Fig. 1, but for model variability associated with varying fr_0 at constant V_m. Parameter values: $fr_0 \in [17.5, 70]$ (light to dark); $V_m = 55\,\mathrm{m\,s^{-1}}$. (a) Nondimensional angular momentum. (b) Wind speed for $r_0 \in [350, 1400]$ at constant $f = 5 \times 10^{-5}\,\mathrm{s^{-1}}$. (c) Wind speed for $f \in [2.5, 10] \times 10^{-5}\,\mathrm{s^{-1}}$ at constant $r_0 = 700\,\mathrm{km}$. Solution shown in blue is common to both this figure and Fig. 1. All $\tilde{M}$ curves converge by definition to (1, 1).

variability in $\tilde{M}$ space (V_m, fr_0). The first wind field mode corresponds to variation in the inner-core structure associated with changes in intensity V_m relative to a fixed overall size. Physically, increases in intensity correspond to an inward progression of angular momentum surfaces that need not extend beyond some finite radius. Equivalently, this mode may correspond to an induced variation in r_m (which varies V_m indirectly), such as in an eyewall replacement cycle, in which convection forced at a radius larger than r_m generates a secondary wind maximum and concomitant weakening of the original wind maximum (Sitkowski et al. 2011).[2] The second wind field mode corresponds to variation in overall size r_0, such that the entire wind field is implicitly rescaled

[2] The model in its current form does not support multiple wind maxima.

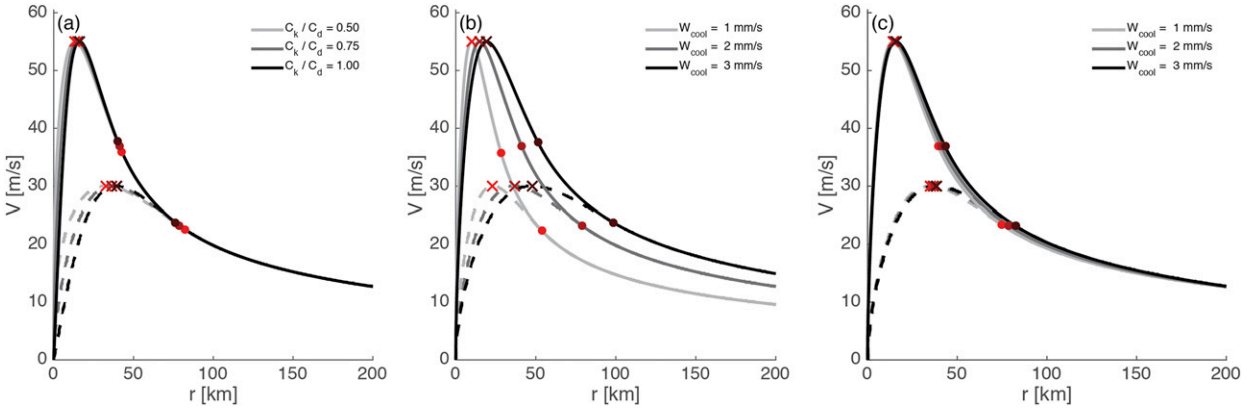

FIG. 3. Sensitivity of the model wind field to environmental parameters, for a high-intensity case ($V_m = 55\,\mathrm{m\,s^{-1}}$) and a low-intensity case $V_m = 30\,\mathrm{m\,s^{-1}}$ with $r_0 = 700\,\mathrm{km}$ and $f = 5\times10^{-5}\,\mathrm{s^{-1}}$. (a) Sensitivity to C_k/C_d. (b) Sensitivity to W_{cool}. (c) As in (b), but fit to $r_{12} = 218.4\,\mathrm{km}$, corresponding to $r_0 = 700\,\mathrm{km}$ for $W_{\mathrm{cool}} = 2\,\mathrm{mm\,s^{-1}}$. Light to dark shading in order of increasing parameter magnitude. Markers denote r_m (crosses) and r_a (dots).

(nonuniformly) according to the physics of the structural model. Physically, the same intensity may be achieved at different sizes, as the inward progression of surfaces of angular momentum may occur at any angular momentum magnitude. This mode also aligns with canonical potential intensity theory (Emanuel 1986), in which r_0 may be taken as a free parameter (below the upper-bound scaling V_p/f, where V_p is the potential intensity). Finally, the third wind field mode corresponds to a subtler variation in structure relative to a fixed overall size associated with changes in latitude f. Taken together, the structure of the wind field depends on all three parameters, while size of the wind field is independent and fully encapsulated in the single parameter r_0. Moreover, the nature of this model dictates that r_0 is a fundamental measure of storm size, both because r_0 defines the magnitude of the initial source of angular momentum for the system (for a given value of f) M_0 from which the storm circulation is ultimately derived, and because it is a component of the parameter fr_0 in the outer structure model itself.

Finally, we briefly explore the sensitivity of the model wind field to the two environmental parameters. Figure 3 displays a set of solutions for a characteristic tropical cyclone at both higher intensity ($V_m = 55\,\mathrm{m\,s^{-1}}$) and lower intensity ($V_m = 30\,\mathrm{m\,s^{-1}}$) for $f = 5\times10^{-5}\,\mathrm{s^{-1}}$ and $r_0 = 700\,\mathrm{km}$. We vary C_k/C_d and W_{cool} over the plausible ranges [0.5, 1] and [1, 3] $\mathrm{mm\,s^{-1}}$, respectively. First, Fig. 3a displays the sensitivity to C_k/C_d, which is confined to the inner solution (i.e., $r < r_a$) and is relatively weak, with $r_m \in [13.4, 16.2]\,\mathrm{km}$ for the higher-intensity case and $r_m \in [32.7, 39.3]\,\mathrm{km}$ for the lower-intensity case. This weak sensitivity, which arises from the matching with the outer solution, aligns with the findings of Bryan (2012) of near-zero sensitivity of r_m to C_k/C_d in numerical model simulations. Note that the inner-core wind field remains relatively similar across this parameter space, as the broadening of the wind profile beyond r_m at lower C_k/C_d partially offsets the simultaneous inward shift; the primary sensitivity is in the precise radius where the wind profile actually attains its peak value. Second, Fig. 3b displays the sensitivity to W_{cool}, which is stronger and affects the solution at all radii. For $C_k/C_d = 0.75$, varying W_{cool} over the plausible range [1, 3] $\mathrm{mm\,s^{-1}}$ yields $r_m \in [9.8, 19.3]\,\mathrm{km}$ for the higher-intensity case and $r_m \in [23.1, 48.0]\,\mathrm{km}$ for the lower-intensity case. However, the underlying sensitivity of the outer solution [Eq. (6)] to W_{cool} is largest at larger radii approaching r_0, such that if the model is specified using an alternative wind radius sufficiently far inside of r_0, the wind profile inside of this radius varies less substantially. For example, Fig. 3c displays the same sensitivity as Fig. 3b but for the solution specified with $r_{12} = 218.4\,\mathrm{km}$ (corresponding to $r_0 = 700\,\mathrm{km}$ for $W_{\mathrm{cool}} = 2\,\mathrm{mm\,s^{-1}}$). The resulting variation in r_m is significantly smaller, spanning $r_m \in [14.3, 15.7]\,\mathrm{km}$ for the higher-intensity case and $r_m \in [35.0, 38.4]\,\mathrm{km}$ for the lower-intensity case. This result has significant practical benefits for the use of information from the outer circulation (e.g., wind radii observations) to infer aspects of the inner core given that the value of W_{cool} carries some uncertainty and may vary in space and time.

3. Comparison with observed variability

We next compare the theoretical modes of variability to observations. We begin with the joint dependence of M_m/M_0 on (V_m, fr_0). We then discuss the modes of wind

field variability and highlight the specific contexts in which these modes typically arise.

a. Data

Observed tropical cyclone wind field variability is quantified principally using the identical HWind-based datasets employed in Part I, which contains a large set of radial profiles of the near-surface ($z = 10$ m) azimuthal wind derived from the raw HWind wind field database (Powell et al. 1998). This dataset is augmented by radial profiles from the QSCAT-R database (Chavas and Vigh 2014), which is based on an optimized version of version 3 of the complete global QuikSCAT dataset (Stiles et al. 2013), also employed in Part I. Uncertainty in wind profile data associated with incomplete spatial data coverage is quantified using a data coverage asymmetry parameter ξ, defined as the normalized magnitude of the vector mean of all grid point distance vectors from center as a function of radius; this quantity spans the range [0, 1], where smaller values of ξ imply greater azimuthal symmetry in data coverage and thus lower uncertainty. The reader is referred to Part I for complete details of these datasets.

Additional analysis of structural covariation is performed using the Extended Best Track dataset (EBT; Demuth et al. 2006) for the North Atlantic and east Pacific basins over the period 1988–2012. EBT provides estimates of r_m, the radii of 64-, 50-, and 34-kt winds (r_{64kt}, r_{50kt}, and r_{34kt}, respectively, in each storm quadrant), and the radius of outermost closed surface isobar r_{OCI} based on observations from aircraft, surface reports (e.g., ships), and satellite imagery. The source data are NHC operational estimates (i.e., not best tracked) prior to 2004 and thereafter are postanalyzed NHC estimates, with the exception of r_m and r_{OCI}, which are not reanalyzed. Though the dataset carries many caveats (Vigh et al. 2012), it has demonstrated value in revealing fundamental relationships between storm structure and evolution (e.g., Carrasco et al. 2014), and ultimately it is by far the most extensive dataset available that contains information about storm radial structure at small and large radii simultaneously with uniform temporal coverage for the full life cycle of all included storms.

b. Angular momentum loss: M_m/M_0

Comparison of the model to observations first requires specification of r_0. In practice, though, r_0 is very difficult to estimate directly from observations because of the combination of the decrease in data coverage and the breakdown of the assumption of constant background flow at large radii (see section 2a for further discussion). Thus, we need to specify an alternative wind radius in its place, preferably one that lies confidently in the nonconvecting outer circulation. We may then estimate r_0 from this wind radius using the outer wind model of Eq. (6), which was shown in Part I to compare very well with observations in the broad outer region of the circulation. Chavas and Emanuel (2010) focused on r_{12}, which offers a balance of sufficient data coverage and minimal noise from both moist convection and variations in the background flow. Here we explore the choice of wind radius by assessing how well the model prediction of r_m (via specification of r_0) compares with HWind observations. Figure 4 displays model performance in its prediction of r_m, as measured by median error, as a joint function of intensity V_m and azimuthal wind speed V_{fit} of the HWind observed wind radius (e.g., r_{12}) to which the model is fit. As in Part I, V_m is defined as the peak HWind azimuthal-mean azimuthal wind. The model is nearly unbiased in its prediction of r_m for V_{fit} in the vicinity of 10–13 m s^{-1}; remarkably, the bias is low for all intensities within the observational range (i.e., up to approximately 55 m s^{-1}). This result matches the finding in Part I that the model with r_m specified was nearly unbiased in predicting wind speeds at large radii (i.e., small wind speeds) across all intensities. Meanwhile, when fitting with intermediate wind speeds, the bias approaches 40%, a reflection of the

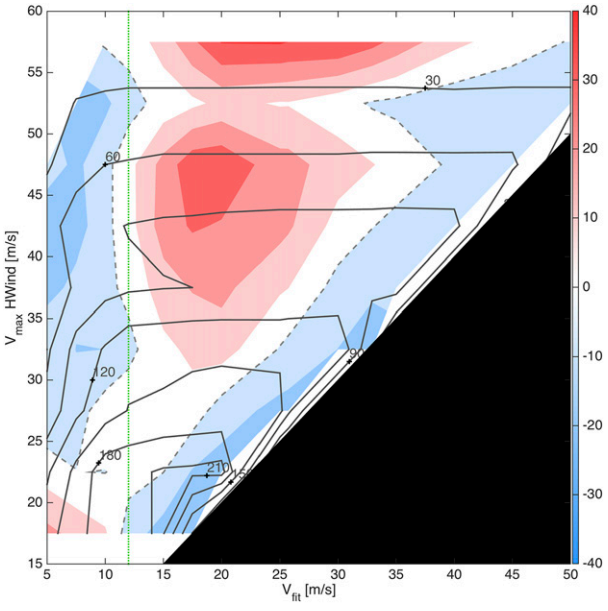

FIG. 4. Median bias {%; defined as $100 \times [(r_{model}/r_{obs}) - 1]$} in the model prediction of r_m as a function of intensity V_m and azimuthal wind speed V_{fit} of the HWind observed wind radius (e.g., r_{12}) to which the model is fit. Contour interval is 10%, and gray dashed line denotes zero bias. Green dotted line denotes r_{12}. Data are grouped into 5 m s^{-1} bins (fill shown for bins with $N \geq 10$); solid black contours denote sample size. Only cases where $\xi < 0.5$ at both r_m and r_{fit} are included.

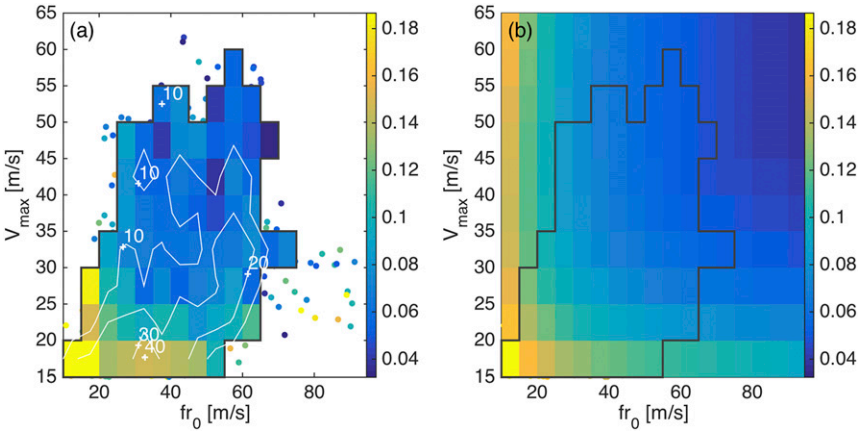

FIG. 5. M_m/M_0 as a joint function of (V_m, fr_0) (a) in observations and (b) predicted by the model. For observations, fill value denotes mean for bins with sample size $N \geq 4$ (white contours denote sample size); individual data shown elsewhere (dots). A small subset of cases exists at large fr_0 and small V_m (not shown). Only cases where $\xi < 0.5$ at both r_m and r_{12} are included. Fill value in (b) denotes value at bin center; black outline matches filled region in (a).

model underestimation of the observed wind profile at intermediate radii demonstrated in Part I for input r_m. Thus, based on these results in combination with the results of Part I, which indicated that the outer model performs very well in reproducing the broad outer circulation when fit to r_{12}, we specify the model using r_{12} from observations in lieu of r_0 (whose value is now given by the model) for the subsequent analysis.

We now compare the theoretical joint dependence of M_m/M_0 on V_m and fr_0 against observations. Figure 5 displays M_m/M_0 as a joint function of V_m and fr_0 for both HWind observations (Fig. 5a; $N = 989$) and the theoretical prediction (Fig. 5b); the observational value of r_0 is estimated from the observed r_{12} using Eq. (6). The majority of the observations span a comparably large range of values of V_m and fr_0 of $[10, 65]$ and $[10, 95]$, respectively, indicating a preference for slightly higher values of fr_0. There exists a small subset of low-intensity cases ($V_m \leq 26\,\mathrm{m\,s^{-1}}$; $N = 8$) possessing values of fr_0 extending to 130. Figure 5 indicates that the theoretical joint dependence of M_m/M_0 on V_m and fr_0 closely matches the observations, with M_m/M_0 decreasing for increasing V_m and fr_0, though the dependence on V_m occurs predominantly at lower intensities as shown in Fig. 1. The close match with the observed joint dependence of M_m/M_0 on V_m and fr_0 indicates that the complete model is doing a credible job capturing the variability of storm structure in nature as a function not only of intensity but of size and latitude as well. To quantify the comparison, we perform a simple multiple linear regression on the logarithm of M_m/M_0 against the logarithms of V_m and fr_0 for all data (i.e., observational value and corresponding model prediction at each data point) where $fr_0 < 75\,\mathrm{m\,s^{-1}}$, which encompasses the filled region in Fig. 5a. Doing so yields best-fit coefficients of -0.56 [95% CI: $(-0.55, -0.58)$] and -0.52 $(-0.51, -0.53)$, respectively, for the model and -0.71 $(-0.61, 0.80)$ and -0.36 $(-0.27, -0.45)$, respectively, for observations; results are quantitatively similar when the regression is applied to the binned data. This result indicates that in the model the conditional dependence on fr_0 is a bit stronger and the conditional dependence on V_m is a bit weaker than in observations. Very similar results are obtained when replacing M_0 with M_{12} (with $M_m/M_{12} \in [0.09, 0.52]$ for the filled region shown in Fig. 5a), an indication that the dependence on fr_0 is not confined solely to the far outer region between r_{12} and r_0. Note that the precise value of M_m/M_0 shown in Fig. 5b, which is essentially an integral over the entire predicted wind structure, will be sensitive to the choice of r_{12} as our outer wind radius as well as the two environmental parameters, but the existence and general character of this joint dependence are not.

There may be a temptation in Eq. (9) and Fig. 5 to nondimensionalize both velocity parameters by V_p in order to transform the two storm-specific parameters into storm intensity and outer size each normalized by their respective theoretical upper bounds, V_p and V_p/f (Emanuel 1995b). However, from Eq. (6), doing so requires the equivalent nondimensionalization of W_{cool}/C_d, thereby undercutting our assumption that this parameter follow a fixed functional form in space and time, a step that simplifies the analysis. Such a nondimensionalization would lead directly to the result of Chavas and Emanuel (2014), which demonstrated that r_0 at equilibrium scales primarily with V_p/f and secondarily

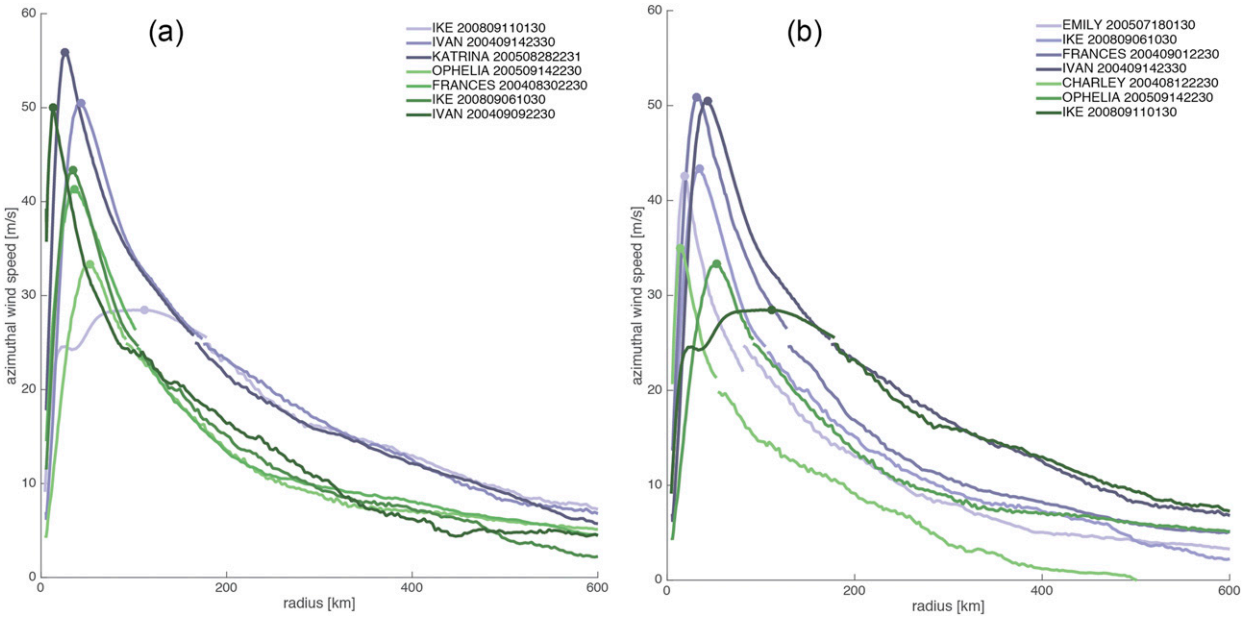

FIG. 6. Examples of observed wind field variability, from subset of cases with combined HWind and QuikSCAT data (cf. Fig. 3 of Part I) where HWind data are used for $r < r_{25}$. (a) Variability in intensity at approximately constant outer size, for subsets of cases at a smaller size (green) and a larger size (blue); light to dark shading is in order of increasing V_m. (b) Variability in size at approximately constant intensity, for subsets of cases at a lower intensity (green) and a higher intensity (blue); light to dark shading is in order of increasing r_{12}. Markers denote r_m and V_m. Legend denotes storm name and analysis date and time.

with the nondimensional parameter $C_d V_p / W_{\text{cool}}$. Real storms in nature appear to be far from equilibrium, though, as r_0 in observations is known to span a wide range of sizes and does not appear to scale in any simple manner with this equilibrium length scale (Chavas et al. 2016). Thus, the model as presented here applies whether or not r_0 is equilibrated, as it makes no assumption about the scaling of r_0 but rather simply externalizes it into a free parameter. As such, the model dictates that the complete radial structure of the tropical cyclone wind field is dependent upon the absolute storm intensity and absolute size while remaining conditionally independent of the environmental parameter V_p. We note from Fig. 5a, though, that the range of values of fr_0 for reasonably intense storms ($V_m > 35\ \text{m s}^{-1}$) is nearly identical to that of V_m ($V_m < 65\ \text{m s}^{-1}$; $fr_0 < 70\ \text{m s}^{-1}$); given that V_p bounds V_m from above (i.e., $V_m \leq V_p$) in observations (Emanuel 2000), this leads to $fr_0 \leq V_p$ and thus $r_0 \leq V_p/f$, indicating that V_p/f may successfully represent an absolute length scale for the upper bound on r_0 in nature as predicted by theory.

c. *Wind field variability*

The three modes of wind field variability have direct relationships to observed variability in nature. Below we explore the observed behavior of the wind field, with particular emphasis on the contrasting modes of variability that prevail within the storm life cycle (intrastorm) and across storms (interstorm).

1) INTENSITY AND OUTER SIZE

We begin with a general exploration of how the observed wind field tends to vary. First, to demonstrate examples, Fig. 6 shows a small subset of wind profiles that possess nearly concurrent HWind data for the inner region and QuikSCAT data out to large radii (cf. Fig. 3 of Part I). These wind profiles display two modes of wind field variability: variability in intensity at approximately constant outer size, at both a smaller and a larger size (Fig. 6a), and variability in size at approximately constant intensity, at both a lower and a higher intensity (Fig. 6b). In the former, the broad outer circulation is remarkably similar across cases in the presence of large variations in V_m and an associated contraction of r_m with increasing intensity. This behavior reflects the theoretical mode of variability characterized by varying V_m at fixed (r_0, f) (Fig. 1b). In the latter, the wind fields possess very similar qualitative structures, but which exist at different sizes. This behavior reflects the theoretical mode of variability characterized by varying r_0 at fixed (V_m, f) (Fig. 2b).

Moreover, wind field variability due to variation in intensity represents the principle mode within the storm life cycle, whereas that due to variation in size represents the principle mode across storms. From the broader

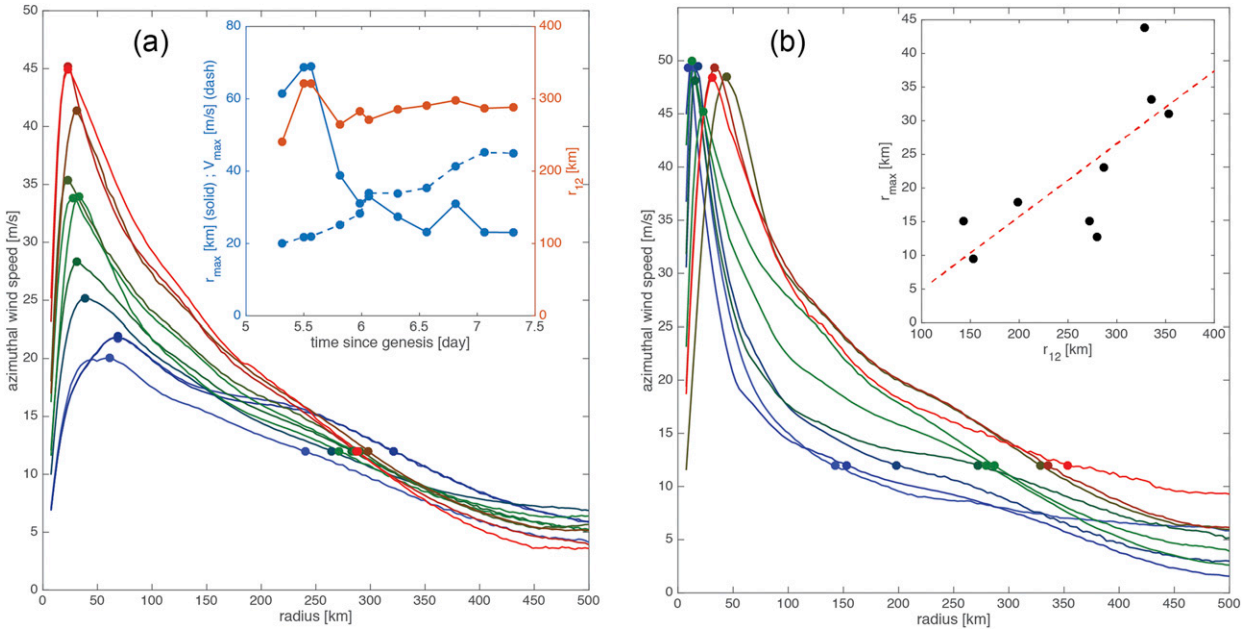

FIG. 7. Examples of observed wind field variability within and across storms, from the HWind database. (a) Variability in structure due to intensification, illustrated by the time evolution of the radial profile of the azimuthal wind for Hurricane Earl (2010) over a 2-day period of intensification (time increases from blue to green to red for the period 0730 UTC 29 Aug to 0730 UTC 31 Aug); inset displays time evolution of V_m (blue dashed), r_m (blue solid), and r_{12} (orange). (b) Variability in size, illustrated by the subset of radial profiles across storms in which $V_m \in [45, 50]\,\mathrm{m\,s^{-1}}$ and f restricted to below 20°N (r_{12} increases from blue to green to red; one profile per storm); inset displays correlation between r_m and r_{12}. Markers denote r_m and r_{12}.

HWind database, Fig. 7 displays observed variability in the radial profile of the azimuthal wind. First, Fig. 7a shows wind profiles for Hurricane Earl (2010) during a 2-day period of significant intensification. Within an 18-h window from 0730 UTC 29 Aug to 0130 UTC 30 Aug, V_m increases from 20 to 34 $\mathrm{m\,s^{-1}}$ and then more gradually to 45 $\mathrm{m\,s^{-1}}$ over the subsequent 24 h. During this period, f changes minimally as Earl traverses from 16.8° to 20.2°N. Intensification is accompanied by a corresponding marked decrease in r_m from 69 to 23 km within a 24-h period; meanwhile, the outer wind field remains largely unperturbed throughout, with r_{12} remaining approximately constant at 300 km. Wind speeds at intermediate radii beyond r_m ($r \in [100, 200]$ km) continue to increase with intensification, in contrast to the observed cases in Fig. 6a and the model behavior in Fig. 1b in which the wind field only in the vicinity of r_m varies with changes in V_m. This difference reflects the statistical underestimation of observed wind speeds by the model at intermediate radii found in Part I, suggesting that this behavior may be specific to the time-dependent processes associated with intensification itself (Stern et al. 2015). Overall, this intrastorm variability reflects the theoretical mode of variability associated with changes in intensity in Fig. 1. Second, Fig. 7b shows the subset of wind profiles for which $V_m \in [45, 50]\,\mathrm{m\,s^{-1}}$ across all storms in the HWind database (one profile per storm, corresponding to the highest available V_m within the bin) and at latitudes below 20°N to limit the variability in f ($3.5\text{–}4.9 \times 10^5\,\mathrm{s^{-1}}$). For nearly constant intensity and comparable latitude, storms exist across a range of sizes, with r_m (9.5–43.8 km) and r_{12} (142.6–353.6 km) now covarying strongly together. Overall, this interstorm variability reflects the theoretical mode of variability associated with changes in size in Fig. 2. Note that the two modes may occasionally occur simultaneously within the storm life cycle; indeed, the two instances of Hurricane Ike (2008) in Fig. 6 indicate joint variability in intensity and size (specifically, weakening and expansion) during the intervening 5-day period.

Building on these examples, we now extend this analysis of wind field covariation to the full HWind database to assess the extent to which these two modes emerge statistically over many storms. Figure 8a displays the Kendall rank correlation matrix disaggregated into intrastorm and interstorm components among V_m, four canonical operational wind radii (r_m, $r_{64\mathrm{kt}}$, $r_{50\mathrm{kt}}$, $r_{34\mathrm{kt}}$), and r_{12}; we require $\xi \leq 0.5$ at a given wind radius to be considered valid. All quantities are calculated from the azimuthal-mean azimuthal wind profile. Intrastorm correlation is defined as the mean over all storms of the correlation calculated for each storm, while interstorm

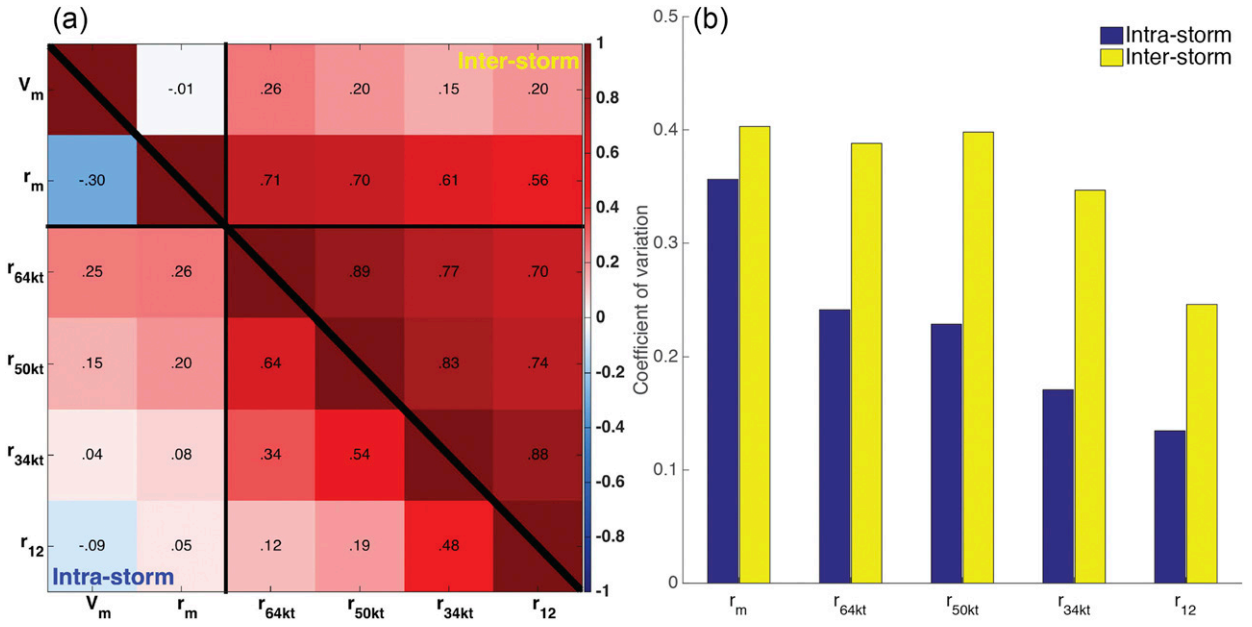

FIG. 8. Statistics of wind field covariation for the HWind database. (a) Rank correlation matrix for (bottom-left half) intrastorm and (top-right half) interstorm variability among canonical wind radii. Thin black lines separate quantities commonly associated with the inner core (V_m, r_m) and outer region (r_{64kt}, r_{50kt}, r_{34kt}, r_{12}), though the intermediate radii may occasionally be located in the inner core when found close to r_m. (b) CV (σ/μ) of each wind radius for intra- and interstorm variability. For all data, sample size defined as storms with at least five time steps with valid data for all six parameters ($N = 19$); only those time steps with valid data for all parameters are included in the analysis. Intrastorm data defined as mean of set of storm-specific correlations/CVs; interstorm data defined as correlation/CV calculated from set of parameter values averaged over life cycle of each storm. Only wind radii where $\xi < 0.5$ are included.

correlation is the correlation of the parameter values averaged over the life cycle of each storm. The sample is defined as storms with at least five time steps with valid data for all six parameters to ensure a robust dataset for analysis ($N = 19$ storms); only those time steps with valid data for all parameters are included in the analysis. The parameters of Fig. 8 are categorized into the inner core (V_m, r_m) and the outer region (r_{64kt}, r_{50kt}, r_{34kt}, r_{12}) although the intermediate wind radii may occasionally lie in the inner core when the corresponding wind speed is comparable to the storm intensity. Furthermore, Fig. 8b quantifies the magnitude of intrastorm and interstorm variability via the coefficient of variation (CV; σ/μ) of each wind radius for this sample. For further corroboration, we apply this analysis identically to the much more extensive Extended Best Track database for the combined Atlantic (1988–2012) and east Pacific (2001–12) basins (Fig. 9), where r_{OCI} replaces r_{12} as the outermost wind radius. The sample is defined as storms with at least 10 time steps with valid data for all six parameters ($N = 144$ storms); the larger size of the EBT dataset allows for a stricter time step threshold, though results are quantitatively similar when using the same threshold as in Fig. 8. Azimuthal-mean values of r_{64kt}, r_{50kt}, and r_{34kt} are each defined as the mean value across all quadrants with valid data, and values within each quadrant correspond to the maximum extent of the respective wind speed. As discussed below, both datasets give very similar results regarding the nature of wind field variability.

Within the storm life cycle, V_m and r_m are negatively correlated, as follows from the characteristic reduction of r_m with intensification discussed above. The inner and outer regions covary very weakly as found by Weatherford and Gray (1988) and also demonstrated in the analysis of Part I, as the covariance among the outer-region wind radii in the HWind database is strong but decreases in magnitude moving radially inward. For example, r_{12} covaries strongly with r_{34kt} and successively less strongly with r_{50kt} and r_{64kt} until the correlation approaches zero with r_m. For EBT data, a similar pattern emerges, though the covariance between r_{34kt} and r_{OCI} is weaker than that between r_{34kt} and r_{12} in HWind. We note that r_{OCI} and r_{12} are not equivalent, as r_{OCI} does not translate easily to any particular wind radius owing in part to the sensitivity of its estimation to environmental pressure and the flow-dependent effects on closed isobars, as well as its lack of postevent reanalysis. Finally, the coefficient of variation, representing the magnitude of intrastorm variability, decreases steadily as one

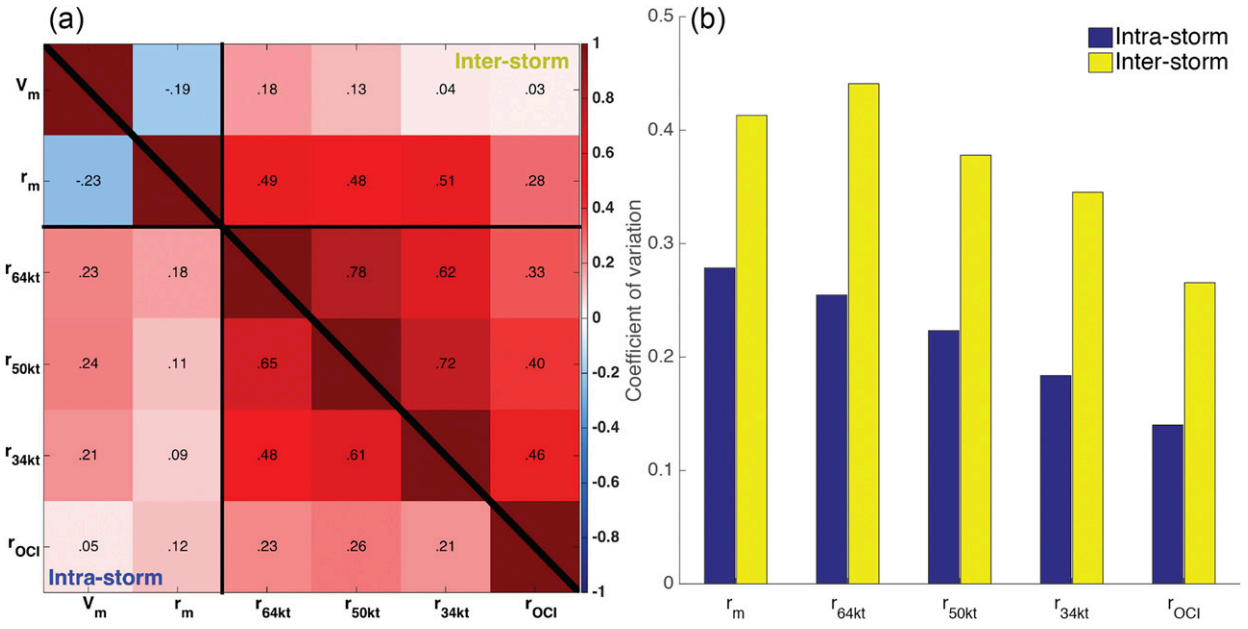

FIG. 9. As in Fig. 8, but for the Extended Best Track dataset for the combined Atlantic (1988–2012) and east Pacific (2001–12). Radius of outermost closed isobar r_{OCI} replaces r_{12}. Sample size defined as storms with at least 10 time steps with valid data for all six parameters ($N = 144$). Azimuthal-mean values of r_{64kt}, r_{50kt}, and r_{34kt} are each defined as the mean value across all quadrants with valid data.

moves radially outward, reaching a minimum value of 0.13 and 0.14 for intrastorm variability of r_{12} (HWind) and r_{OCI} (EBT), respectively, indicative of the stability of the outer region relative to the turbulent inner core.

Meanwhile, across storms, two key distinctions emerge. First, r_m covaries strongly with all outer radii and, moreover, all outer-region wind radii covary strongly and uniformly with one another, an indication that the radial extent of the entire storm varies in unison. The correlation between r_m and the outer radii is a bit stronger in HWind than in EBT. Second, the magnitude of the variability of all radial length scales beyond r_m is much larger than in the intrastorm case. This result is also found for EBT r_m but is less evident for HWind r_m —the latter likely a more reliable r_m dataset. Indeed, r_m may exhibit equivalent magnitudes of variability both within and across storms. These results corroborate the finding of Chavas and Emanuel (2010) noting the much larger variance of storm size across storms as compared to within the storm life cycle. Additionally, r_m and V_m across storms are not correlated in the HWind database but they covary negatively across storms in the EBT database (Fig. 8a); this difference may again reflect the fact that r_m is not reanalyzed in EBT. This lack of a correlation between r_m and V_m likely indicates that the magnitude of interstorm variability in storm size overwhelms any signal from the characteristic anticorrelated variability of r_m and V_m found in the intrastorm case, as has been noted in prior studies (e.g., Stern and Nolan 2009; Stern et al. 2014). Indeed, the requirement of valid data for r_{64kt} imposes the constraint that $V_m \geq 64$ kt, thereby limiting the variability of V_m; relaxing the requirement of valid data for all HWind parameters simultaneously gives an interstorm correlation between V_m and r_m of -0.40.

For the EBT analysis, results are similar when applied to the Atlantic and east Pacific databases separately (not shown). However, the east Pacific basin exhibits smaller variation in the outer radii, as measured by CV, particularly across storms (though interstorm values remain consistently larger than intrastorm values), as well as a significantly stronger correlation between outer size metrics and V_m (though not r_m) both within and across storms. The former may reflect the consistently smaller storm sizes found in the east Pacific basin (Avila and Pasch 1995; Chavas and Emanuel 2010; Knaff et al. 2014; Chavas et al. 2016). The reason for the latter is not known, though may be tied simply to a lack of in situ data coverage relative to the Atlantic basin. Further analysis of interbasin differences is left for future work.

Finally, we return to the HWind database to quantitatively compare these two modes of variability specifically in the context of r_m in observations and predicted by the model for input r_{12}. We calculate correlation coefficients between modeled and observed r_m for all data as well as for intrastorm and interstorm data (as in Figs. 8 and 9). For all data combined, modeled and observed values of r_m correlate strongly, with a Pearson correlation coefficient of $r = 0.76$ (Kendall rank

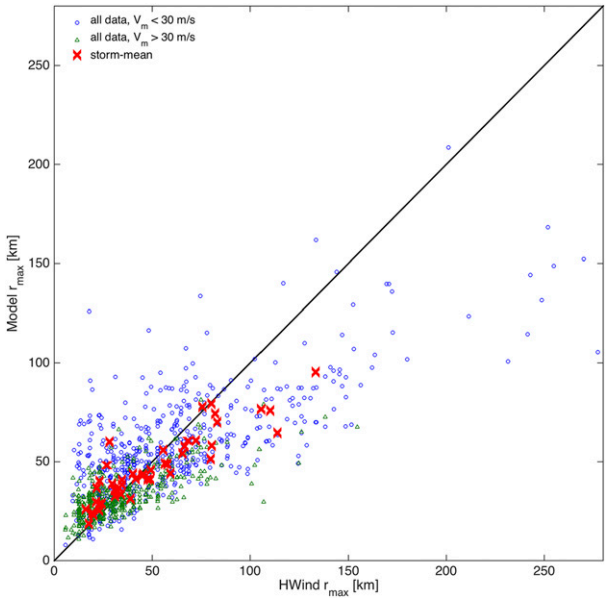

FIG. 10. Scatterplot comparing HWind r_m and model prediction for all data with $V_m < 30\,\mathrm{m\,s^{-1}}$ (blue circle; $N = 559$) and $V_m > 30\,\mathrm{m\,s^{-1}}$ (green triangle; $N = 430$), as well as interstorm data (red cross; $N = 46$), defined as the mean over the storm life cycle for storms with at least five valid observed and modeled values. Only data with $\xi < 0.5$ at both r_m and r_{12} are included.

correlation $r = 0.53$). For the sample of storms with at least five time steps with valid values for observed and modeled r_m ($N = 46$ storms), the intrastorm Pearson correlation coefficient between HWind r_m and the model prediction is $r = 0.52$ (Kendall rank coefficient $r = 0.35$), while that for the interstorm case is $r = 0.90$ (Kendall rank coefficient $r = 0.74$). These relationships are illustrated in Fig. 10, which shows a scatterplot of the observed and modeled r_m for all data, split into a lower-intensity group ($V_m < 30\,\mathrm{m\,s^{-1}}$) and a higher-intensity group ($V_m > 30\,\mathrm{m\,s^{-1}}$), as well as for the interstorm data. Though correlation values indicate that the model is capable of capturing a substantial fraction of the observed variance in r_m, particularly across storms, the model increasingly underestimates r_m at larger values of r_m (both overall and storm mean) above approximately 60 km. This behavior occurs for both the lower- and higher-intensity groups, suggesting that the bias is associated with size itself, as the model simply performs less well for large values of r_m. Indeed, linear regression between model and observed values of r_m yields a slope of 0.48 for all data and 0.55 for storm-mean data (y-intercept values of 22.5 and 19.4 km, respectively). This result corroborates the aforementioned finding that the model sensitivity of M_m/M_0 to fr_0 and V_m is stronger and weaker, respectively, than in observations, as r_m would be expected to be larger for, for example, a storm with smaller V_m and/or larger r_0 at fixed f. As with the prediction of M_m/M_0, the precise prediction of r_m from an outer radius entails an integral over the entire structure and thus is sensitive to all components and parameters as well as the chosen metric for outer size. Such considerations must be accounted for in potential operational applications, which are discussed in section 5. Note that the weaker intrastorm correlation within the storm life cycle is perhaps unsurprising given that intrastorm variability essentially represents short-time-scale covariation, particularly between r_m and V_m relative to a stable outer circulation and thus is sensitive to the noisy turbulent processes in the inner core. Meanwhile, interstorm variability represents the spatial component of covariation, particularly between r_m and r_{12}, whose time average will act to smooth out this noise.

2) LATITUDE

The third mode of wind field variability f is more subtle, in terms of both the much smaller magnitude of its effect on the wind field (Fig. 2) as well as the smaller observed variability of f in nature. Nonetheless, the combination of Eq. (6) and Fig. 5 suggests that the effect of variable f on storm structure is real, though its effects on the wind field are not easily isolated in the observational database given that canonical storm tracks occupy a relatively narrow latitude band and, moreover, storms that move poleward are prone to substantial changes in intensity and size given the climatological decrease of potential intensity and increase in probability of extratropical interaction with latitude. Additionally, the potential for dependence of r_0 on f itself (Chavas and Emanuel 2014; Khairoutdinov and Emanuel 2013; Held and Zhao 2008; Knaff et al. 2014) may undercut the existence of this as a truly independent mode of wind field variability in nature.

Here we highlight one observational example in Fig. 11, which displays the structural evolution of Hurricane Earl (2010) in a 2-day period shortly after that displayed in Fig. 7. As shown in Fig. 11a, Earl moved gradually poleward by 10° latitude while maintaining a relatively constant intensity during this period. Figure 11b displays the observed and model predicted time series of M_m/M_0, where the value of r_0 used to calculate the observational value of M_0 is estimated from r_{12} using the outer model [Eq. (6)]. The model correctly captures the decrease in M_m/M_0 with increasing f during this period. Moreover, the time series of r_{12}, which exhibits a statistically significant upward linear trend, suggests that the storm is expanding as it moves poleward, reflecting the positive correlation between size and latitude that has been noted in past research (Merrill 1984; Mueller et al. 2006; Knaff et al. 2014). However, Fig. 11c also shows that the

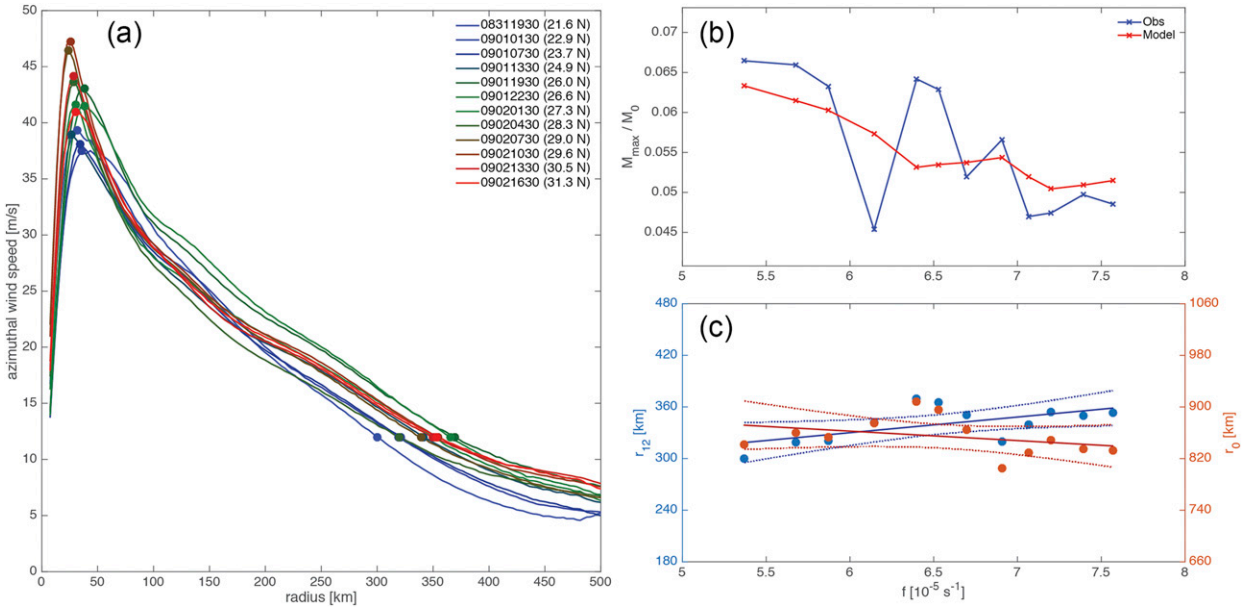

FIG. 11. Example of observed variability in structure due to changes in latitude for Hurricane Earl (2010) from HWind data. (a) Time evolution of the radial profile of the azimuthal wind during a 2-day period of poleward motion (time and latitude increase from blue to green to red for the period 1930 UTC 31 Aug to 1630 UTC 2 Sep); markers denote r_m and r_{12}. Legend denotes analysis date and time and storm-center latitude. (b) Variation of M_m/M_0 with f in observations (blue) and predicted by the model (red). (c) Variation of r_{12} (cyan) and r_0 (orange) with f for the same time period, with linear trend (solid) and 95% confidence interval (dashed).

increase in r_{12} translates to a constant or perhaps slightly decreasing trend in r_0, a consequence of the fact that the outer region model dictates that the distance between r_0 and r_{12} decreases with increasing f. As a matter of practical significance, this example demonstrates how the analysis of variation in size depends crucially on the metric of interest—here the observed size metric r_{12} appears to be increasing whereas the size of the entire circulation is not. Taken together, this example highlights the subtle changes in storm structure that accompany an increase in latitude: the circulation at intermediate radii (e.g., r_{12}) expands relative to a stable r_0.

Overall, this case study provides some indication that the wind field is only weakly sensitive to variations in f for values spanning the typical tropical main development region, in line with the model prediction (Fig. 2c). Further insight may be gained by evaluating the role of temporal variability in f on the storm wind field in an idealized modeling setting, but this effort is beyond the scope of this work. Experiments under a simplified axisymmetric geometry are appealing, though the strong dependence of storm structure and intensity on the radial turbulent mixing length (Chavas and Emanuel 2014) complicates the interpretation of the effect of variable f. Modeling experiments in three dimensions, in which the effects of the radial turbulent mixing length are limited only to subgrid-scale processes may offer a fruitful way forward.

4. Implications for understanding and modeling the tropical cyclone wind field

First and foremost, the model presents a viable conceptual framework for defining the oft-conflated terms "size" and "structure" and their respective variabilities. The model successfully externalizes r_0 as an independent parameter, thereby defining size simply as the absolute length scale r_0 and structure as the wind field relative to r_0 (i.e., $\partial M/\partial r$ or $\partial V/\partial r$), the latter given by the combination of two theoretical solutions and their respective parametric dependencies. Note that, though size (i.e., r_0) is independent of structure, structure is not independent of size because of the dependence of the outer structure model on fr_0. A similar conceptual hypothesis for wind field variability was proposed by Holland and Merrill (1984) (Fig. 1 therein) in the context of changes in intensity and size though absent the dependence of the entire radial profile on variations in size.[3] Here, variation in size r_0 occurs in conjunction with the model's radial structure, such that changes in r_0 implicitly rescale (nonuniformly) the entire radial profile in accordance with the model physics. Such behavior aligns with the observed tendency for storms in nature to

[3] Notably, their definition of "strength" coincidentally corresponds closely to the variability induced by changes in C_k/C_d.

span a large range of sizes while retaining an identical qualitative radial structure. Furthermore, it aligns well with the bed of existing theory for both tropical cyclone intensity and structure that is itself phrased not in terms of absolute radius but rather relative to a single length scale (Emanuel 1995a; Emanuel and Rotunno 2011). We further note that, though one may equivalently specify the wind field solution using an alternative size metric, such as r_m, the emergent behavior of wind field variability is not equivalent. This result arises principally because r_m is correlated with V_m. Indeed, the model presented herein contains additional information regarding wind field variability, particularly structural variability associated with changes in intensity (and perhaps latitude), that is lost when r_m is specified directly.

Second, the standard Cartesian view of the tropical cyclone wind field, which focuses on r_m as the primary structural metric of interest, obscures the more relevant underlying physics of the tropical cyclone wind field based on absolute angular momentum. In particular, intensification is commonly associated with the notion of contraction of the radius of maximum wind, as shown in observations above, and so it is common parlance to define ''contraction'' in Cartesian space as the inward shift of r_m (e.g., Stern et al. 2015). Fundamentally, though, changes in intensity correspond structurally to the contraction of angular momentum surfaces, whose evolution is inherently correlated in radius given that an increase in angular momentum at one point requires an inward flux of angular momentum from larger radius, as discussed in section 1. As such, the conceptual understanding of intensification is best placed in the broader context of variability of the value of angular momentum at r_m (i.e., M_m) relative to its value at some large radius, ideally defined to be at the outer radius (i.e., M_0). From this perspective, M_0 represents the magnitude of the initial source of angular momentum supplied to the system, while the ratio M_m/M_0 represents the fraction of this initial magnitude that remains at r_m and depends on intensity, size, and latitude. The canonical view of the contraction of r_m itself is simply the special (but common) case of variation in V_m at fixed f and r_0, in which M_m varies (and angular momentum surfaces contract) relative to a fixed value of M_0 (i.e., Fig. 1). However, M_0 may also vary simultaneously owing to, for example, an increase in size r_0, whose effect on r_m may offset that of contraction. Though this behavior may lead to the perception that contraction of r_m is not occurring (e.g., Stern et al. 2015), instead it may simply reflect the independent and simultaneous effects of contraction with intensification and overall expansion on the time tendency of r_m. A strict focus on r_m alone will miss this distinction. Thus, the model presented herein defines the wind field through the lens of angular momentum, whose variability can be understood theoretically and from which quantities of practical interest such as r_m may be extracted. We note, however, that the above discussion does not exclude r_m as an important physical length scale, as there are known inner-core phenomena, such as eyewall replacement cycles and other boundary layer processes (e.g., Kepert and Nolan 2014) as well as frictional dissipation and entropy production (e.g., Khairoutdinov and Emanuel 2013), that likely depend specifically on r_m.

Third, from a mechanistic perspective, local increases in angular momentum require inward import from larger radii. This highlights the critical role of radial fluxes of angular momentum in the boundary layer, which has received substantial attention in size and structure research (e.g., Chan and Chan 2013, 2014), particularly in the context of secondary eyewall formation (e.g., Abarca and Montgomery 2014; Kepert 2013). However, it is worth noting that in the context of this model, the information used to define the equilibrium distribution of angular momentum at all radii has its source not from within the boundary layer but rather from above it: the inner-region distribution depends on the nature of turbulence in the outflow at the top of the troposphere, while the outer-region distribution depends on the rate at which free-tropospheric air subsides under the influence of radiative cooling. As such, angular momentum fluxes are undoubtedly critical in the boundary layer yet are slaved to processes occurring outside of it. The implication is that an exclusive focus on the boundary layer alone, while potentially very useful for understanding time-dependent processes such as secondary eyewall formation, may miss connections with the free troposphere, particularly at equilibrium. This perspective may provide insight into how storm–environment interaction, including spiral rainbands and variations in ambient moisture (e.g., Xu and Wang 2010; Hill and Lackmann 2009), may further modulate storm structure.

Fourth, additional insight may be gained by considering the relevant equilibration time scales at play. The model can be considered to have five components: three input parameters (V_m, r_0, and f) and two structural elements given by the solutions for the inner and outer regions. Theoretically, four of these elements operate on fast time scales of less than 1 day. First, V_m is governed energetically by the dynamics of ventilation theory (Tang and Emanuel 2010) [as well as upper-ocean turbulent mixing (Price 1981)] whose time scale is $O(<1)$ day (Tang and Emanuel 2012; Emanuel 2012), and indeed observations and models clearly indicate that V_m is

prone to changing rapidly (Kaplan et al. 2010). Second, f carries a dynamical adjustment time scale given by its reciprocal [$O(<1)$ day], which is itself much faster than the time scale of variation in f, given by $f/v_t\beta = O(10)$ days for characteristic values of $\beta = \partial f/\partial y$ at latitude $\phi = 20°$ and storm meridional translation speed $v_t = 3\,\mathrm{m\,s^{-1}}$. Third, the inner structural model is governed by the physics of Kelvin–Helmholtz turbulence in the outflow and the subsequent inward propagation of information from the outflow to the boundary layer by gravity waves, both of which carry very fast time scales of $O(1)$ h (Lignieres et al. 1999). Finally, the outer structural model is governed largely by the physics of the Ekman layer, whose equilibration time scale is $O(<1)$ day and that is typically unperturbed during the life cycle evolution of a given storm. In contrast, the final element r_0 has been shown in an idealized model to carry very slow equilibration time scales of $O(10)$ days (Chavas and Emanuel 2014) and is known observationally to vary relatively slowly during the storm life cycle (Chavas and Emanuel 2010; Knaff et al. 2014). However, no theoretical time scale exists for its dynamics, and the equilibrium length scale for r_0, given by the ratio V_p/f (Chavas and Emanuel 2014), is insufficient to explain its substantial variation in nature (Chavas et al. 2016). This separation of time scales indicates that, in contrast to size, storm structure may be viably represented by an equilibrium model, such as the one presented here, on time scales relevant for observations and operational forecasting.

Finally, the model's decomposition of wind field variability conveniently enables the credible representation of a fully specified, time-dependent physical solution for the wind field whose variability is encapsulated in the parameters V_m, r_0, and f. Given our theoretical understanding of the physics and dynamics of V_m in the context of environmental ventilation (Tang and Emanuel 2010, 2012), and given information on storm track, the lone remaining requirement is an external model for the free parameter r_0 (i.e., storm size). Note that in principle, M_0 could replace r_0 as the relevant free parameter. However, such an approach implicitly combines f and r_0, whereas r_0 is often taken to be a random variable (e.g., Lin et al. 2014), while the distribution of f is independently set by the genesis regions and storm tracks of a given climate state. Indeed, variation in M_0 is dominated by that of r_0 owing to the large variance of r_0 in nature (Chavas et al. 2016; Knaff et al. 2014) relative to the smaller variance in f associated with the narrow tropical storm track, an effect that is amplified by the quadratic dependence on r_0. Nonetheless, understanding the potential relationship between f and r_0, indicative principally of the dependence of precursor disturbance size on latitude, is a worthy research endeavor.

5. Summary and conclusions

Part I of this work developed a simple theoretical model for the complete radial structure of the low-level absolute angular momentum, and thus azimuthal wind field, in a tropical cyclone, one that carries two options for its specification: the maximum wind speed and radius of maximum wind, or the maximum wind speed and the outer radius of vanishing wind. The former was shown to compare well quantitatively to a large database of wind profiles from observed tropical cyclones in nature. However, information about the nature of wind field variability is implicitly embedded in the external parameters V_m and r_m. Physical models for V_m exist, but not for r_m, whose representation is hampered by its inherently noisy nature as well as the lack of a holistic understanding of the wind field and its variability.

Here we find that the alternative model specification, which takes r_0 as input and r_m as output, offers significant additional insight into the nature of wind field variability when viewed through the lens of absolute angular momentum. Such an approach also carries theoretical appeal by considering variations in absolute angular momentum relative to its value at the source radius. A nondimensional form of the model predicts the ratio of the angular momentum at the radius of maximum wind and the outer radius M_m/M_0 to be a function of four parameters: two storm-specific velocity scales, V_m and fr_0, whose space–time variability is large, and two environmental parameters, C_k/C_d in the inner region and W_{cool}/C_d in the outer region, whose space–time variability is small. Variability of the two storm-specific parameters translate to three distinct modes of wind field variability due to changes in intensity, size, and latitude, where size is defined as r_0. The theoretical joint dependence of M_m/M_0 on V_m and fr_0 is shown to closely match observations when given the radius of a wind speed in the vicinity of $12\,\mathrm{m\,s^{-1}}$ (r_{12}), indicating that the model successfully captures the principal dependence of storm structure on intensity, size, and latitude found in nature. The corresponding modes of wind field variability in the model appear to compare well with observations, in particular 1) the intrastorm variability of the inner-core structure due to intensification/decay relative to a stable outer circulation and 2) the interstorm variability in storm size. More broadly, the model offers theoretical and conceptual insight into the nature of the tropical cyclone wind field, including the oft-conflated terms "size" (r_0) and "structure" (the wind field relative to r_0; i.e., $\partial M/\partial r$ or $\partial V/\partial r$) and their distinct

modes of variability. In particular, the model dictates that size is independent of structure, but structure is not independent of size, as the solution "feels" r_0 at all radii as a result of the dependence on fr_0 in the outer solution.

Considering both parts of this work in combination, the model makes various predictions, whose successes and limitations we wish to review here. We begin with model successes:

- The model provides a credible representation of the complete radial structure of the tropical cyclone, characterized by an inner ascending region and an outer descending region that are directly juxtaposed. The result constitutes an overturning circulation consistent with the known physics of tropical cyclones.
- The model captures the qualitative behavior of the radial structure of the wind field, including rapid decay beyond r_m (represented by the inner solution) and a long tail of gradual decay at larger radii (represented by the outer solution). In particular, the outer solution is capable of quantitatively reproducing the broad outer circulation of observed storms, which constitutes the majority of the areal coverage of the storm.
- The model defines wind field variability, including the terms size and structure, through the fundamental lens of absolute angular momentum. Outer size r_0 represents the radius of the initial source of absolute angular momentum for the storm imparted by Earth's rotation. Structure represents the inward rate of loss of angular momentum relative to its initial value at r_0.
- The model predicts that the structural quantity M_m/M_0 depends jointly on V_m and fr_0, matching observations.
- By externalizing intensity and outer size as free parameters, the model predicts that intensity and size may vary independently, consistent with behavior in numerical models and observations.
- The model predicts that r_m depends principally on both intensity and outer size, consistent with behavior in numerical models and observations.
- The model predicts, for an increase in intensity at fixed size and latitude, the contraction of both r_m and the convecting inner core relative to a stable outer circulation, consistent with behavior in numerical models and observations.
- The model predicts the (nonuniform) rescaling of the entire wind field associated with changes in size at fixed intensity and latitude, consistent with behavior in numerical models and observations.
- The model predicts a slow expansion of the wind field at small and intermediate radii for increasing f, consistent with observations.
- The model's underlying time scales suggest that storm structure equilibrates rapidly relative to changes in intensity and size, matching the common qualitative structure over a range of observed intensities and sizes found in this analysis.

Notably, the above successes are not dependent on precise estimates of the model's parameter values. Nonetheless, limitations of the model remain, particularly for precise quantitative predictions:

- Though reasonably well constrained by both the performance of the outer solution and independent theoretical and modeling results, the value for the radiative-subsidence rate is still subject to uncertainty in the details of its calculation (as well as unknown space–time variability). Meanwhile, the value of C_k/C_d is poorly constrained, and the intensity dependence of its best-fit values do not match existing observational estimates though the range of values is the correct order of magnitude (cf. Part I). Uncertainties in both parameters may mask model deficiencies, though the qualitative behavior of the model does not depend on their precise values.
- The inner solution neglects myriad real-world effects (e.g., dissipative heating, the pressure dependence of the saturation enthalpy, supergradient winds) and its underlying physics otherwise cannot be validated here. Ultimately, the inner solution is a simple and useful model for a complex region, though other more suitable theories cannot be excluded.
- The model statistically underestimates the wind field at intermediate radii for reasonably strong storms. This behavior is hypothesized to arise from a transition region of intermittent rainfall at intermediate radii, such as spiral rainbands, that is not captured by the model, though other explanations or model deficiencies may be at play.
- The precise quantitative prediction of M_m/M_0 (and thus r_m) represents an integral over the complete radial structure and thus may be sensitive to the choice of values for the environmental parameters, W_{cool} and C_k/C_d, as well as the input metric for outer size.
- The predicted dependence of wind field behavior on latitude is not conclusively testable from observations alone.
- Transient inner-core structural variability, such as eyewall replacement cycles, is not accounted for.
- The role of the boundary layer is left unaddressed here, particularly in the inner core. The successes of the model suggest that the boundary layer plays only a secondary role in the general behavior of the wind field at least for the nonconvecting outer region.

These limitations indicate many potential avenues for improvement. Overall, though, the model compares

well to nature in its ability to reproduce not only the characteristic radial structure itself but also the dominant modes of wind field variability within and across storms, including fundamental relationships linking the angular momentum at the radius of maximum wind to that at the outer radius. In this way, the whole is greater than the sum of its parts: the complete model is more than merely a juxtaposition of solutions for the inner and outer regions, as information is also encoded in the interplay of the solutions that arises from their juxtaposition. Moreover, the system may be interpreted to behave like a vortex within a vortex, where the inner vortex sustains itself off of absolute angular momentum supplied by the outer vortex and the outer vortex sustains itself off of angular momentum supplied by the rotating Earth; the outer vortex is necessary only to achieve global mass balance in the form of the overturning circulation. The result is a credible model for the complete, time-dependent wind field whose evolution depends principally on three parameters—intensity, size, and rotation rate—each of which must be modeled externally.

Finally, from a practical perspective, the equilibration time scales of the model components suggest that variability of storm structure in nature on time scales relevant to operational forecasting may be credibly captured by equilibrium dynamics. As such, the model offers the potential to place individual wind radii within a holistic, physics-based framework for the tropical cyclone wind field that considers their interdependent variability. For example, the interpretation of an observed increase in r_m (e.g., ''weakening,'' ''expansion,'' ''structure change'') depends on the concurrent changes in intensity, size, and latitude, each of which will have distinct effects on the covariation of r_m with other observed wind radii (e.g., r_{34kt}). Moreover, one convenient aspect of this model is its capacity to utilize information from the outer region of the storm to predict inner-core structure, a property not without precedent in the parametric hurricane wind modeling literature (Holland et al. 2010). Indeed, though r_m is a perfectly suitable metric of storm size if appropriate data are available, a measure of the outer circulation may be a useful substitute, as it may be easier to estimate observationally and tends not to vary substantially with time nor with V_m. For example, intensity and storm-center location are provided by operational forecast centers and a measure of outer storm size could be routinely obtained from satellite (scatterometry, GPS reflection, or IR), which together could be input to provide an estimate of r_m. Precise prediction of operationally relevant quantities from available observations, though, requires careful consideration, including accounting for model uncertainties. Alternatively, changes in the radius of maximum wind, such as an expansion induced by an eyewall replacement cycle (Maclay et al. 2008), could be monitored from the outside when inner-core observations are unavailable. Last, the climatology of r_0 can be applied, as a substitute of the climatology of r_m, in quantifying the risk of associated hazards, such as storm surge (Lin et al. 2014). Such potential applications to operational forecasting and risk analysis may be explored in future work.

Acknowledgments. The authors thank Kerry Emanuel for valuable feedback in the early stages of this work. Special thanks to Dr. Daniel Stern, Dr. John Knaff, and one anonymous reviewer for their valuable feedback that greatly improved this manuscript. We also thank Mark Powell for his work developing the HWind database and CIRA RAMMB at CSU for their work developing and maintaining the Extended Best Track database. This material is based on work supported by the National Science Foundation (NSF) under Award AGS-1331362 and the National Oceanic and Atmospheric Administration (NOAA), U.S. Department of Commerce, under Award NA14OAR4320106. The statements, findings, conclusions, and recommendations are those of the authors and do not necessarily reflect the views of NSF, NOAA, or the U.S. Department of Commerce.

REFERENCES

Abarca, S. F., and M. T. Montgomery, 2014: Are eyewall replacement cycles governed largely by axisymmetric balance dynamics? *J. Atmos. Sci.*, **71**, 3723–3738, doi:10.1175/JAS-D-14-0018.1.

Avila, L. A., and R. J. Pasch, 1995: Atlantic tropical systems of 1993. *Mon. Wea. Rev.*, **123**, 887–896, doi:10.1175/1520-0493(1995)123<0887:ATSO>2.0.CO;2.

Bryan, G. H., 2012: Effects of surface exchange coefficients and turbulence length scales on the intensity and structure of numerically simulated hurricanes. *Mon. Wea. Rev.*, **140**, 1125–1143, doi:10.1175/MWR-D-11-00231.1.

Carrasco, C. A., C. W. Landsea, and Y.-L. Lin, 2014: The influence of tropical cyclone size on its intensification. *Wea. Forecasting*, **29**, 582–590, doi:10.1175/WAF-D-13-00092.1.

Chan, K. T., and J. C. Chan, 2012: Size and strength of tropical cyclones as inferred from QuikSCAT data. *Mon. Wea. Rev.*, **140**, 811–824, doi:10.1175/MWR-D-10-05062.1.

——, and ——, 2013: Angular momentum transports and synoptic flow patterns associated with tropical cyclone size change. *Mon. Wea. Rev.*, **141**, 3985–4007, doi:10.1175/MWR-D-12-00204.1.

——, and ——, 2014: Impacts of initial vortex size and planetary vorticity on tropical cyclone size. *Quart. J. Roy. Meteor. Soc.*, **140**, 2235–2248, doi:10.1002/qj.2292.

——, and ——, 2015: Global climatology of tropical cyclone size as inferred from QuikSCAT data. *Int. J. Climatol.*, **35**, 4843–4848, doi:10.1002/joc.4307.

Chavas, D. R., and K. A. Emanuel, 2010: A QuikSCAT climatology of tropical cyclone size. *Geophys. Res. Lett.*, **37**, L18816, doi:10.1029/2010GL044558.

——, and K. Emanuel, 2014: Equilibrium tropical cyclone size in an idealized state of axisymmetric radiative–convective equilibrium. *J. Atmos. Sci.*, **71**, 1663–1680, doi:10.1175/JAS-D-13-0155.1.

——, and J. Vigh, 2014: QSCAT-R: The QuikSCAT tropical cyclone radial structure dataset. NCAR Tech. Note TN-513+STR, 27 pp. [Available online at http://nldr.library.ucar.edu/repository/assets/technotes/TECH-NOTE-000-000-000-882.pdf.]

——, N. Lin, and K. Emanuel, 2015: A model for the complete radial structure of the tropical cyclone wind field. Part I: Comparison with observed structure. *J. Atmos. Sci.*, **72**, 3647–3662, doi:10.1175/JAS-D-15-0014.1.

——, ——, W. Dong, and Y. Lin, 2016: Observed tropical cyclone size revisited. *J. Climate*, **29**, 2923–2939, doi:10.1175/JCLI-D-15-0731.1.

DeMaria, M., and J. Kaplan, 1994: A Statistical Hurricane Intensity Prediction Scheme (SHIPS) for the Atlantic basin. *Wea. Forecasting*, **9**, 209–220, doi:10.1175/1520-0434(1994)009<0209:ASHIPS>2.0.CO;2.

Demuth, J. L., M. DeMaria, and J. A. Knaff, 2006: Improvement of Advanced Microwave Sounding Unit tropical cyclone intensity and size estimation algorithms. *J. Appl. Meteor. Climatol.*, **45**, 1573–1581, doi:10.1175/JAM2429.1.

Donelan, M., B. Haus, N. Reul, W. Plant, M. Stiassnie, H. Graber, O. Brown, and E. Saltzman, 2004: On the limiting aerodynamic roughness of the ocean in very strong winds. *Geophys. Res. Lett.*, **31**, L18306, doi:10.1029/2004GL019460.

Emanuel, K. A., 1986: An air–sea interaction theory for tropical cyclones. Part I: Steady-state maintenance. *J. Atmos. Sci.*, **43**, 585–605, doi:10.1175/1520-0469(1986)043<0585:AASITF>2.0.CO;2.

——, 1995a: The behavior of a simple hurricane model using a convective scheme based on subcloud-layer entropy equilibrium. *J. Atmos. Sci.*, **52**, 3960–3968, doi:10.1175/1520-0469(1995)052<3960:TBOASH>2.0.CO;2.

——, 1995b: Sensitivity of tropical cyclones to surface exchange coefficients and a revised steady-state model incorporating eye dynamics. *J. Atmos. Sci.*, **52**, 3969–3976, doi:10.1175/1520-0469(1995)052<3969:SOTCTS>2.0.CO;2.

——, 2000: A statistical analysis of tropical cyclone intensity. *Mon. Wea. Rev.*, **128**, 1139–1152, doi:10.1175/1520-0493(2000)128<1139:ASAOTC>2.0.CO;2.

——, 2004: Tropical cyclone energetics and structure. *Atmospheric Turbulence and Mesoscale Meteorology*, E. Fedorovich, R. Rotunno, and S. B., Eds., Cambridge University Press, 165–192.

——, 2012: Self-stratification of tropical cyclone outflow. Part II: Implications for storm intensification. *J. Atmos. Sci.*, **69**, 988–996, doi:10.1175/JAS-D-11-0177.1.

——, and R. Rotunno, 2011: Self-stratification of tropical cyclone outflow. Part I: Implications for storm structure. *J. Atmos. Sci.*, **68**, 2236–2249, doi:10.1175/JAS-D-10-05024.1.

Held, I. M., and M. Zhao, 2008: Horizontally homogeneous rotating radiative–convective equilibria at GCM resolution. *J. Atmos. Sci.*, **65**, 2003–2013, doi:10.1175/2007JAS2604.1.

Hill, K. A., and G. M. Lackmann, 2009: Influence of environmental humidity on tropical cyclone size. *Mon. Wea. Rev.*, **137**, 3294–3315, doi:10.1175/2009MWR2679.1.

Holland, G. J., and R. T. Merrill, 1984: On the dynamics of tropical cyclone structural changes. *Quart. J. Roy. Meteor. Soc.*, **110**, 723–745, doi:10.1002/qj.49711046510.

——, J. I. Belanger, and A. Fritz, 2010: A revised model for radial profiles of hurricane winds. *Mon. Wea. Rev.*, **138**, 4393–4401, doi:10.1175/2010MWR3317.1.

Kaplan, J., M. DeMaria, and J. A. Knaff, 2010: A revised tropical cyclone rapid intensification index for the Atlantic and eastern North Pacific basins. *Wea. Forecasting*, **25**, 220–241, doi:10.1175/2009WAF2222280.1.

Kepert, J. D., 2013: How does the boundary layer contribute to eyewall replacement cycles in axisymmetric tropical cyclones? *J. Atmos. Sci.*, **70**, 2808–2830, doi:10.1175/JAS-D-13-046.1.

——, and D. S. Nolan, 2014: Reply to comments on how does the boundary layer contribute to eyewall replacement cycles in axisymmetric tropical cyclones? *J. Atmos. Sci.*, **71**, 4692–4704, doi:10.1175/JAS-D-14-0014.1.

Khairoutdinov, M., and K. Emanuel, 2013: Rotating radiative-convective equilibrium simulated by a cloud-resolving model. *J. Adv. Model. Earth Syst.*, **5**, 816–825, doi:10.1002/2013MS000253.

Knaff, J. A., and R. M. Zehr, 2007: Reexamination of tropical cyclone wind–pressure relationships. *Wea. Forecasting*, **22**, 71–88, doi:10.1175/WAF965.1.

——, S. P. Longmore, and D. A. Molenar, 2014: An objective satellite-based tropical cyclone size climatology. *J. Climate*, **27**, doi:10.1175/JCLI-D-13-00096.1.

Knutson, T., J. Sirutis, M. Zhao, R. Tuleya, M. Bender, G. Vecchi, G. Villarini, and D. Chavas, 2015: Global projections of intense tropical cyclone activity for the late twenty-first century from dynamical downscaling of CMIP5/RCP4.5 scenarios. *J. Climate*, **28**, 7203–7224, doi:10.1175/JCLI-D-15-0129.1.

Kossin, J. P., J. A. Knaff, H. I. Berger, D. C. Herndon, T. A. Cram, C. S. Velden, R. J. Murnane, and J. D. Hawkins, 2007: Estimating hurricane wind structure in the absence of aircraft reconnaissance. *Wea. Forecasting*, **22**, 89–101, doi:10.1175/WAF985.1.

Lee, C.-S., K. K. Cheung, W.-T. Fang, and R. L. Elsberry, 2010: Initial maintenance of tropical cyclone size in the western North Pacific. *Mon. Wea. Rev.*, **138**, 3207–3223, doi:10.1175/2010MWR3023.1.

Lignieres, F., F. Califano, and A. Mangeney, 1999: Shear layer instability in a highly diffusive stably stratified atmosphere. arXiv.org, 11 pp. [Available online at http://arxiv.org/abs/astro-ph/9908184.]

Lin, N., P. Lane, K. A. Emanuel, R. M. Sullivan, and J. P. Donnelly, 2014: Heightened hurricane surge risk in northwest Florida revealed from climatological-hydrodynamic modeling and paleorecord reconstruction. *J. Geophys. Res. Atmos.*, **119**, 8606–8623, doi:10.1002/2014JD021584.

Maclay, K. S., M. DeMaria, and T. H. Vonder Haar, 2008: Tropical cyclone inner-core kinetic energy evolution. *Mon. Wea. Rev.*, **136**, 4882–4898, doi:10.1175/2008MWR2268.1.

Merrill, R. T., 1984: A comparison of large and small tropical cyclones. *Mon. Wea. Rev.*, **112**, 1408–1418, doi:10.1175/1520-0493(1984)112<1408:ACOLAS>2.0.CO;2.

Mueller, K. J., M. DeMaria, J. Knaff, J. P. Kossin, and T. H. Vonder Haar, 2006: Objective estimation of tropical cyclone wind structure from infrared satellite data. *Wea. Forecasting*, **21**, 990–1005, doi:10.1175/WAF955.1.

Powell, M. D., S. H. Houston, L. R. Amat, and N. Morisseau-Leroy, 1998: The HRD real-time hurricane wind analysis system. *J. Wind Eng. Ind. Aerodyn.*, **77–78**, 53–64, doi:10.1016/S0167-6105(98)00131-7.

Price, J. F., 1981: Upper ocean response to a hurricane. *J. Phys. Oceanogr.*, **11**, 153–175, doi:10.1175/1520-0485(1981)011<0153:UORTAH>2.0.CO;2.

Reed, K. A., and D. R. Chavas, 2015: Uniformly rotating global radiative-convective equilibrium in the Community

Atmosphere Model, version 5. *J. Adv. Model. Earth Syst.*, **7**, 1938–1955, doi:10.1002/2015MS000519.

Rotunno, R., and G. H. Bryan, 2012: Effects of parameterized diffusion on simulated hurricanes. *J. Atmos. Sci.*, **69**, 2284–2299, doi:10.1175/JAS-D-11-0204.1.

Sitkowski, M., J. P. Kossin, and C. M. Rozoff, 2011: Intensity and structure changes during hurricane eyewall replacement cycles. *Mon. Wea. Rev.*, **139**, 3829–3847, doi:10.1175/MWR-D-11-00034.1.

Smith, R., 1980: Tropical cyclone eye dynamics. *J. Atmos. Sci.*, **37**, 1227–1232, doi:10.1175/1520-0469(1980)037<1227:TCED>2.0.CO;2.

Stern, D. P., and D. S. Nolan, 2009: Reexamining the vertical structure of tangential winds in tropical cyclones: Observations and theory. *J. Atmos. Sci.*, **66**, 3579–3600, doi:10.1175/2009JAS2916.1.

——, J. R. Brisbois, and D. S. Nolan, 2014: An expanded dataset of hurricane eyewall sizes and slopes. *J. Atmos. Sci.*, **71**, 2747–2762, doi:10.1175/JAS-D-13-0302.1.

——, J. L. Vigh, D. S. Nolan, and F. Zhang, 2015: Revisiting the relationship between eyewall contraction and intensification. *J. Atmos. Sci.*, **72**, 1283–1306, doi:10.1175/JAS-D-14-0261.1.

Stiles, B. W., R. E. Danielson, W. L. Poulsen, M. J. Brennan, S. Hristova-Veleva, T.-P. Shen, and A. G. Fore, 2013: Optimized tropical cyclone winds from QuikSCAT: A neural network approach. *IEEE Trans. Geosci. Remote Sens.*, **52**, 7418–7434, doi:10.1109/TGRS.2014.2312333.

Tang, B., and K. Emanuel, 2010: Midlevel ventilation's constraint on tropical cyclone intensity. *J. Atmos. Sci.*, **67**, 1817–1830, doi:10.1175/2010JAS3318.1.

——, and ——, 2012: A ventilation index for tropical cyclones. *Bull. Amer. Meteor. Soc.*, **93**, 1901–1912, doi:10.1175/BAMS-D-11-00165.1.

Vigh, J. L., J. A. Knaff, and W. H. Schubert, 2012: A climatology of hurricane eye formation. *Mon. Wea. Rev.*, **140**, 1405–1426, doi:10.1175/MWR-D-11-00108.1.

Weatherford, C., and W. Gray, 1988: Typhoon structure as revealed by aircraft reconnaissance. Part I: Data analysis and climatology. *Mon. Wea. Rev.*, **116**, 1032–1043, doi:10.1175/1520-0493(1988)116<1032:TSARBA>2.0.CO;2.

Xu, J., and Y. Wang, 2010: Sensitivity of the simulated tropical cyclone inner-core size to the initial vortex size. *Mon. Wea. Rev.*, **138**, 4135–4157, doi:10.1175/2010MWR3335.1.